Iranian Journal of Numerical Analysis and Optimization
Vol. ??, No. ??, ??, pp ??
https://doi.org/??
https://ijnao.um.ac.ir/

CC BY NC

Research Article

Multiphysics and uncertainty-aware dynamic modeling of pico-hydrokinetic turbine systems with wake effects

C. Kikmo Wilba*, E.R. Yannick and J.P. Ngoma

Abstract

We develop a unified multiphysics modeling framework for pico-hydrokinetic turbine systems operating under variable inflow conditions and parametric uncertainties. The proposed formulation couples the incompressible Navier–Stokes equations, a reduced-order rotor dynamics model, and an electrical conversion subsystem, leading to a consistent PDE-ODE system that captures the interaction between hydrodynamic forcing, mechanical rotation, and energy extraction. We reformulate the global dynamics as an evolution problem in a Hilbert phase space, where the coupled system is governed by a structured operator combining nonlinear hydrodynamic effects, mechanical-electrical coupling, and wake-induced velocity deficit mechanisms. In this setting, we embed a Jensen-type actuator-disk representation directly into the

*Corresponding author

Received 2 February 2026; revised 3 June 2026; accepted 10 June 2026

Christophe Kikmo Wilba
National Higher Polytechnic School of Douala, University of Douala, Cameroon.
e-mail: christopherkikmo@gmail.com

Ekani Roger Yannick
National Higher Polytechnic School of Douala, University of Douala, Cameroon.
e-mail: tassotiyannick@yahoo.com

Jean Pierr Ngoma
National Higher Polytechnic School of Douala, University of Douala, Cameroon.
e-mail: ngoma8273@gmail.com

How to cite this article
Kikmo Wilba, C., Yannick, E.R. and Ngoma, J.P. , Multiphysics and uncertainty-aware dynamic modeling of pico-hydrokinetic turbine systems with wake effects . *Iran. J. Numer. Anal. Optim.*, ??; ??(??): ??-??. ??

evolution equations, ensuring a dynamic and self-consistent description of wake effects within the fluid-structure interaction loop. We incorporate uncertainties in inflow conditions and model parameters through a parametric formulation, enabling sensitivity-oriented analysis of system behavior under nonideal operating regimes. We then introduce a structure-preserving discretization strategy based on finite-dimensional monotone approximation and backward Euler time integration, ensuring consistency with the underlying operator structure. Our main contribution is the derivation of a coherent operator-theoretic framework that integrates fluid, mechanical, electrical, and wake dynamics into a single mathematically structured evolution system, providing a foundation for both analytical investigations and reduced-order numerical simulation of pico-hydrokinetic energy conversion systems.

AMS subject classifications (2020): 76-10, 65C20, 65K10, 90C26.

Keywords: Multiphysics modeling; Hydrokinetic turbines; PDE-ODE coupling; Monotone operators; Wake modeling; Uncertainty quantification; Reduced-order models; Numerical validation.

1 Introduction

The global transition toward sustainable energy systems requires the development of scalable and decentralized renewable technologies capable of meeting increasing demand while reducing greenhouse gas emissions. In this context, hydrokinetic energy, which extracts power directly from flowing water without the need for large hydraulic infrastructures, represents a promising and environmentally compatible solution. In particular, small-scale and pico-hydrokinetic turbines are well suited for deployment in rivers, canals, and tidal currents, especially in remote or off-grid regions. Despite their potential, the operation of such systems in natural open-channel environments raises significant modeling challenges. These include strong spatial and temporal variability of the flow, complex fluid-structure interactions, and sensitivity to environmental uncertainties. As a result, the development of predictive and physically consistent models is essential for understanding system behavior and supporting design and optimization processes.

A variety of modeling approaches have been proposed in the literature. Simplified actuator disk models, such as the classical formulation introduced by Jensen [8], provide a tractable representation of wake effects and are widely used in both wind and hydrokinetic energy studies. While these models offer useful qualitative insights and low computational cost, they rely on restrictive assumptions, including uniform velocity distributions and simplified wake expansion laws. Consequently, they are not well suited for capturing transient dynamics or detailed flow-

structure interactions. More advanced approaches incorporate hydrodynamic effects through reduced-order models or computational fluid dynamics (CFD) simulations [22, 13, 3]. These methods improve physical realism but are often limited in scope, focusing either on the fluid dynamics alone or on isolated aspects of turbine performance. In many cases, the coupling between fluid flow, rotor dynamics, and electrical energy conversion is treated in a simplified or partially decoupled manner [16, 24]. Furthermore, uncertainty in environmental conditions, such as inflow variability and parameter fluctuations, is typically addressed through empirical adjustments rather than being systematically embedded in the governing equations.

Another limitation of existing studies lies in the level of mathematical structure supporting the proposed models. Although concepts from dynamical systems or functional analysis are sometimes invoked, the associated assumptions and their implications are not always clearly articulated, particularly for coupled systems involving partial differential equations (PDEs) and ordinary differential equations (ODEs) [12, 25, 14]. As a consequence, analytical properties such as well-posedness or stability are often discussed in a formal or heuristic manner.

The present work aims to address these limitations by proposing a coherent multiphysics modeling framework for pico-hydrokinetic turbine systems, balancing physical relevance and analytical consistency. The approach combines (i) an incompressible flow model based on the Navier–Stokes equations, (ii) a reduced-order mechanical model describing rotor dynamics, and (iii) a simplified representation of electrical power generation. Particular attention is devoted to the modeling of wake effects through an actuator-disk-inspired formulation. In contrast with standard static implementations, this representation is explicitly embedded within the coupled dynamical system, allowing for a consistent interaction between wake-induced velocity deficits and turbine dynamics. The objective is not to introduce a fundamentally new wake law, but rather to integrate existing modeling ideas into a unified and interpretable framework.

Environmental and parametric uncertainties are incorporated through a structured parametric description, enabling a qualitative assessment of their influence on system dynamics. The analytical treatment is developed in a manner consistent with established results for incompressible flows and dynamical systems. Under appropriate regularity and compatibility assumptions, the coupled system is formulated within a functional framework that clarifies its mathematical structure. The results are therefore to be understood as providing a consistent and structured analysis, rather than a complete or fully rigorous theory for all regimes. Within this setting, the main contributions of the present study can be summarized as follows:

- We derive an explicit coupled PDE-ODE model for a pico-hydrokinetic turbine, combining an incompressible Navier–Stokes description of the flow, a low-order mechanical model of the rotor, and a lumped electrical subsystem within a single evolution framework.

- We reformulate the resulting multiphysics dynamics as a monotone operator problem in a Hilbert phase space, identify the relevant m-accretive blocks, and state well-posedness and stability properties under clearly articulated structural assumptions.

- We embed a simplified, Jensen-type wake representation directly into the coupled evolution system, so that wake-induced velocity deficits, rotor motion, and electrical conversion are treated in a consistent dynamical setting rather than as static corrections.

- We propose an operator-theoretic spatial and temporal discretization and perform a benchmark against a reduced reference model and published hydrokinetic performance data, in order to assess the coherence of the simplified wake modeling and of the coupled PDE-ODE formulation.

In addition, a numerical strategy is outlined to illustrate the dynamical response of the coupled system and to assess the coherence of the model with expected physical behavior. The emphasis is placed on interpretability and consistency, with the aim of supporting future developments toward more detailed simulations and experimental validation. It is important to emphasize that the present study does not provide a full quantitative validation of the model against experimental measurements or high-fidelity CFD benchmarks for pico-hydrokinetic turbines. In particular, detailed comparisons with measured wake profiles and turbine performance curves, as reported in dedicated experimental and design studies, lie beyond the scope of this work and are left for future investigation. The remainder of the paper is organized as follows. Section 3 introduces the physical configuration and modeling assumptions. Section 4 presents the coupled multiphysics formulation and the analytical properties of the system within a consistent functional setting. Section 5 outlines the numerical approach and provides illustrative simulations, including the benchmark and validation procedure. Section 6 discusses the results and modeling choices, and section 7 concludes the paper with perspectives for future work.

2 Governing equations of the coupled system

We consider an incompressible viscous fluid flowing in a bounded domain $\Omega \subset \mathbb{R}^3$ of class $C^{1,1}$, representing an open-channel configuration with inflow and outflow boundaries. The fluid interacts with a rigid-axis turbine rotor and an attached electrical circuit. The primary unknowns are the fluid velocity $\boldsymbol{u}(x,t)$ and pressure $p(x,t)$, the rotor angular position $\theta(t)$ and angular velocity $\omega(t)$, and the electrical current $i(t)$ and voltage $v(t)$.

2.1 Fluid subsystem

The fluid dynamics are governed by the incompressible Navier–Stokes equations:

$$\begin{cases} \rho\,\partial_t \boldsymbol{u} + \rho(\boldsymbol{u}\cdot\nabla)\boldsymbol{u} - \nu\Delta\boldsymbol{u} + \nabla p = \boldsymbol{f}_{\text{ext}} + \boldsymbol{f}_{\text{rot}}(\omega) & \text{in } \Omega\times(0,T), \\ \nabla\cdot\boldsymbol{u} = 0 & \text{in } \Omega\times(0,T). \end{cases} \tag{1}$$

The boundary $\partial\Omega$ is decomposed as $\partial\Omega = \Gamma_{\text{in}} \cup \Gamma_{\text{out}} \cup \Gamma_{\text{wall}}$, where

- on the inflow boundary Γ_{in}, a velocity profile is prescribed:

$$\boldsymbol{u} = \boldsymbol{u}_{\text{in}} \quad \text{on } \Gamma_{\text{in}}\times(0,T),$$

- on the outflow boundary Γ_{out}, a stress-free (do-nothing) condition is imposed:

$$(-p\mathbf{I} + \nu\nabla\boldsymbol{u})\boldsymbol{n} = 0 \quad \text{on } \Gamma_{\text{out}}\times(0,T),$$

- on the solid walls Γ_{wall}, the no-slip condition holds:

$$\boldsymbol{u} = 0 \quad \text{on } \Gamma_{\text{wall}}\times(0,T).$$

The initial condition is given by

$$\boldsymbol{u}(\cdot,0) = \boldsymbol{u}_0 \quad \text{in } \Omega,$$

with $\boldsymbol{u}_0$ divergence-free. The forcing term $\boldsymbol{f}_{\text{rot}}(\omega)$ models the action of the turbine on the flow. It is interpreted as a distributed body force, consistent with actuator-disk-type approximations, and is assumed to depend on ω in a locally Lipschitz manner. This reduced representation is commonly used in hydrokinetic modeling to capture the dominant momentum extraction effects without resolving blade-scale geometry.

2.2 Rotor subsystem

The rotor is modeled as a rigid body rotating about a fixed axis. Its angular dynamics are given by

$$\begin{cases} J\dot{\omega}(t) = T_f(\boldsymbol{u}(t)) - T_e(i(t)) - T_{\text{fric}}(\omega(t)), \\ \dot{\theta}(t) = \omega(t), \end{cases} \quad t \in (0,T). \tag{2}$$

where $J > 0$ denotes the moment of inertia. The hydrodynamic torque $T_f(\boldsymbol{u})$ exerted by the fluid on the rotor is formally defined by

$$T_f(\boldsymbol{u}) := \int_\Gamma \big(\boldsymbol{r} \times \boldsymbol{\sigma}(\boldsymbol{u},p)\boldsymbol{n}\big) \cdot \boldsymbol{e}_\theta \, d\Gamma,$$

where Γ denotes the turbine surface, $\boldsymbol{\sigma}(\boldsymbol{u},p)$ is the Cauchy stress tensor, and $\boldsymbol{r}$ is the position vector. In the weak formulation used later, this torque is understood in a variational sense under suitable regularity assumptions on $\boldsymbol{u}$. For the abstract analysis, it will be represented by a bounded functional $\mathcal{T}_f(\boldsymbol{u})$ defined on the fluid space. The electromagnetic torque is modeled as $T_e(i) = k\, i(t)$, with $k > 0$ a coupling constant. The friction torque is modeled through a maximal monotone graph:

$$T_{\text{fric}}(\omega) \in \partial j(\omega),$$

where $j : \mathbb{R} \to \mathbb{R}$ is a convex function. Typical choices include:

- $j(\omega) = \frac{\mu}{2}\omega^2$ (linear viscous friction),
- or nonsmooth models such as $j(\omega) = \mu|\omega|$.

2.3 Electrical subsystem

The electrical subsystem is modeled by a lumped RLC circuit coupled to the rotor motion:

$$\begin{cases} L\dot{i}(t) + Ri(t) + v(t) = k_m\, \omega(t) + u_{\text{ext}}(t), \\ C\dot{v}(t) + \dfrac{1}{R_L} v(t) - i(t) = 0, \end{cases} \quad t \in (0,T). \tag{3}$$

where L, R, C, and R_L are positive constants. The term $k_m\omega(t)$ represents the electromotive force induced by rotation, and $u_{\text{ext}}(t)$ is an external input. Initial conditions are prescribed as

$$\omega(0) = \omega_0, \quad \theta(0) = \theta_0, \quad i(0) = i_0, \quad v(0) = v_0.$$

2.4 Coupled system and abstract formulation

The coupled system (2)–(3) is closed through the interaction terms $T_f(\boldsymbol{u})$, $T_e(i)$, and $\boldsymbol{f}_{\mathrm{rot}}(\omega)$. Introducing the state vector

$$X(t) := \big(\boldsymbol{u}(\cdot,t), \theta(t), \omega(t), i(t), v(t)\big),$$

the system can be formally recast as an abstract evolution problem in a suitable Hilbert space $\mathcal{H}$:

$$\dot{X}(t) + \mathcal{A}(X(t)) \ni 0, \quad X(0) = X_0.$$

Here, the operator $\mathcal{A}$ collects the Navier–Stokes dynamics, the rotor equations, and the electrical circuit, together with their nonlinear couplings. This formulation provides a unified framework for the analysis of well-posedness and stability developed in the subsequent sections, under assumptions that will be specified precisely later.

2.5 Explicit PDE-ODE coupling and physical interaction mechanisms

The dynamics of the pico-hydrokinetic turbine result from a bidirectional interaction between the incompressible fluid, the rigid-axis rotor, and the lumped electrical circuit. This interaction can be decomposed into three principal mechanisms: (i) fluid forces acting on the rotor blades, (ii) rotor-induced forcing of the fluid, and (iii) electromechanical conversion between mechanical torque and electrical current.

Fluid forces driving the rotor. The hydrodynamic stress $\boldsymbol{\sigma}(\boldsymbol{u}, p)$ on the blade surface $\Gamma \subset \partial\Omega$ induces a net force and torque given by

$$\boldsymbol{F}_f(\boldsymbol{u}, p) := \int_\Gamma \boldsymbol{\sigma}(\boldsymbol{u}, p)\boldsymbol{n}\, d\Gamma, \quad T_f(\boldsymbol{u}, p) := \int_\Gamma \big(\boldsymbol{r} \times \boldsymbol{\sigma}(\boldsymbol{u}, p)\boldsymbol{n}\big) \cdot \boldsymbol{e}_\theta \, d\Gamma.$$

Here $\boldsymbol{n}$ denotes the outward unit normal, $\boldsymbol{r}$ the position vector, and $\boldsymbol{e}_\theta$ the azimuthal direction aligned with the rotor axis. In the reduced model used thereafter, the hydrodynamic torque is represented by a bounded linear functional $T_f(\boldsymbol{u}) = \mathcal{T}_f(\boldsymbol{u})$, acting on the solenoidal velocity space, so that the rotor torque balance (2) closes as

$$J\dot{\omega}(t) = \mathcal{T}_f(\boldsymbol{u}(t)) - T_e(i(t)) - T_{\mathrm{fric}}(\omega(t)).$$

Rotor forcing of the fluid. Conversely, the rotation of the turbine modifies the fluid momentum through an effective body force entering the Navier–Stokes system (2). At the PDE level, the fluid is governed by

$$\rho\,\partial_t \boldsymbol{u} + \rho(\boldsymbol{u}\cdot\nabla)\boldsymbol{u} - \nu\Delta\boldsymbol{u} + \nabla p = \boldsymbol{f}_{\text{ext}} + \boldsymbol{f}_{\text{rot}}(\omega), \quad \nabla\cdot\boldsymbol{u} = 0 \quad \text{in } \Omega\times(0,T),$$

where $\boldsymbol{f}_{\text{rot}}(\omega)$ encodes the turbine-induced forcing. A typical parametrization is $\boldsymbol{f}_{\text{rot}}(\omega(t)) = B(\omega(t))\,\boldsymbol{e}_\theta$, with $B:\mathbb{R}\to\mathbb{R}$ locally Lipschitz, representing momentum extraction and swirl in the turbine region. In the abstract formulation this contribution corresponds to a finite-rank operator

$$\boldsymbol{f}[\omega] := \omega\,P\boldsymbol{\phi}, \quad \boldsymbol{\phi}\in L^2(\Omega)^3,$$

where P is the Leray projector onto divergence-free fields.

Electromechanical conversion and closure. The electrical torque and induced electromotive force couple the rotor with the RLC circuit. We set

$$T_e(i) = k\,i(t), \quad L\dot{i}(t) + Ri(t) + v(t) = k_m\omega(t) + u_{\text{ext}}(t),$$

where $k>0$ and $k_m>0$ are coupling coefficients relating the rotor speed ω to the electrical torque and induced voltage, respectively, and $u_{\text{ext}}(t)$ denotes an external input. The friction torque is modeled via a maximal monotone graph, $T_{\text{fric}}(\omega)\in\partial j(\omega)$, for a convex potential $j:\mathbb{R}\to\mathbb{R}$, for example, $j(\omega)=\frac{\mu}{2}|\omega|$ with $\mu>0$, ensuring a monotone mechanical dissipation mechanism.

Closed PDE-ODE system and abstract operator form. Collecting the fluid equations (2)–(1), the rotor equations (2), and the circuit equations (3), together with the coupling relations for $T_f(\boldsymbol{u})$, $T_e(i)$ and $\boldsymbol{f}_{\text{rot}}(\omega)$, yields a closed PDE-ODE multiphysics system for the state

$$X(t) := \big(\boldsymbol{u}(\cdot,t), \theta(t), \omega(t), i(t), v(t)\big).$$

As shown in section 3, this coupled system admits an equivalent abstract evolution formulation $\dot{X}(t) + \mathcal{A}(X(t)) \ni 0$ in $\mathcal{H}$, where $\mathcal{A}:\mathcal{D}(\mathcal{A})\subset\mathcal{H}\rightrightarrows\mathcal{H}$ is a maximal monotone multiphysics operator combining the Navier–Stokes block, the mechanical rotor block, the electrical block, and their finite-rank couplings. This explicit PDE-ODE coupling provides the physical basis for the operator-theoretic analysis developed in the subsequent sections.

3 Multiphysics monotone phase space

3.1 Open-channel flow configuration and boundary conditions

We consider a three-dimensional open-channel flow configuration representative of a river or canal segment interacting with a pico-hydrokinetic turbine. The fluid domain $\Omega \subset \mathbb{R}^3$ is assumed to be bounded in the transverse and vertical directions, while representing a finite portion of a larger flow system [21, 1, 6]. The boundary $\partial\Omega$ is decomposed as $\partial\Omega = \Gamma_{\text{in}} \cup \Gamma_{\text{out}} \cup \Gamma_{\text{wall}} \cup \Gamma_{\text{free}}$, where Γ_{in} denotes the inflow boundary, Γ_{out} the outflow boundary, Γ_{wall} the solid boundaries (river bed and lateral banks), and Γ_{free} an idealized free surface. In contrast with closed-domain formulations, homogeneous Dirichlet conditions are not imposed on the entire boundary, as this would be physically inconsistent for open-channel flows [1, 6, 19]. Instead, we adopt the following set of boundary conditions:

- Inflow boundary. A prescribed velocity profile is imposed on Γ_{in}: $\mathbf{u} = \mathbf{u}_{\text{in}} \quad \text{on } \Gamma_{\text{in}}$.

- Outflow boundary. A natural ("do-nothing") condition is used on Γ_{out}: $-p\mathbf{n} + \nu\frac{\partial \mathbf{u}}{\partial \mathbf{n}} = \mathbf{0} \quad \text{on } \Gamma_{\text{out}}$, which allows the flow to exit the computational domain without artificial reflections.

- Solid walls. On Γ_{wall}, we impose the no-slip condition: $\mathbf{u} = \mathbf{0} \quad \text{on } \Gamma_{\text{wall}}$, modeling viscous interaction with the channel bed and lateral boundaries.

- Free surface. On Γ_{free}, we consider a simplified stress-free condition: $\mathbf{n} \cdot \boldsymbol{\sigma}(\mathbf{u}, p) = \mathbf{0} \quad \text{on } \Gamma_{\text{free}}$, where $\boldsymbol{\sigma}(\mathbf{u}, p)$ denotes the Cauchy stress tensor. This approximation neglects surface tension and interface deformation and is appropriate for a first-order representation of free-surface effects.

To characterize the flow regime, we introduce the Reynolds number $\text{Re} = \frac{UL}{\nu}$, and, when unsteady effects are considered, the Strouhal number $\text{St} = \frac{L}{UT}$, where U, L, and T denote characteristic velocity, length, and time scales [1]. These dimensionless parameters provide qualitative insight into the relative importance of inertial, viscous, and transient effects.

3.2 Functional framework and multiphysics phase space

We consider divergence-free velocity fields consistent with the above boundary conditions. The solenoidal space is defined by

$$\mathbf{H} := \{\mathbf{u} \in L^2(\Omega)^3 : \nabla \cdot \mathbf{u} = 0\},$$

and the associated energy space by

$$\mathbf{V} = \left\{\mathbf{v} \in H^1(\Omega)^3 : \nabla \cdot \mathbf{v} = 0,\ \mathbf{v}|_{\Gamma_{\text{wall}}} = \mathbf{0}\right\}.$$

Inflow and outflow conditions are incorporated in a weak (variational) sense, which is consistent with open-domain formulations [23]. This leads to the Gelfand triple $\mathbf{V} \hookrightarrow \mathbf{H} \simeq \mathbf{H}^* \hookrightarrow \mathbf{V}'$, with dense and continuous embeddings. We complement the fluid subsystem with finite-dimensional spaces describing the mechanical and electrical components:

$$\mathcal{H}_m := \mathbb{R} \quad \text{(rotor angular velocity)},$$

$$\mathcal{H}_e := \mathbb{R}^2 \quad \text{(electric current } i \text{ and voltage } v\text{)}.$$

The global multiphysics phase space is defined as

$$\mathcal{H} := \mathbf{H} \times \mathcal{H}_m \times \mathcal{H}_e,$$

equipped with the quadratic energy norm

$$\|U\|_{\mathcal{H}}^2 = \|\mathbf{u}\|_{\mathbf{H}}^2 + J\,\omega^2 + L\,i^2 + C\,v^2, \quad U = (\mathbf{u}, \omega, i, v),$$

where J, L, and C are positive physical parameters corresponding to inertia, inductance, and capacitance. This norm can be interpreted as a total energy functional for the coupled system.

3.3 *m*-accretive hydrodynamic block

We introduce the hydrodynamic component of the coupled system. Let $P : L^2(\Omega)^3 \to \mathbf{H}$ denote the Leray projector onto divergence-free vector fields. The Stokes operator is formally defined by $A := -P\Delta$, with a domain implicitly determined through the variational formulation asso-

ciated with the boundary conditions described above. In the present work, we do not rely on a strong characterization of $D(A)$, but rather work within the classical weak solution framework for incompressible flows. The nonlinear convection term is introduced via the trilinear form $b(\mathbf{u}, \mathbf{v}, \mathbf{w}) = \int_\Omega (\mathbf{u} \cdot \nabla)\mathbf{v} \cdot \mathbf{w}\, dx$, which satisfies the standard skew-symmetry property under suitable regularity assumptions.

We define the Navier–Stokes type operator

$$\mathcal{N}(\mathbf{u}) = \nu A\mathbf{u} + B(\mathbf{u}, \mathbf{u}), \quad \mathbf{u} \in \mathbf{V}.$$

The interaction with the turbine is modeled through a distributed forcing term depending on the angular velocity ω:

$$\mathbf{f}[\omega](x) = P\big(g(\omega)\, \boldsymbol{\phi}_{\text{thrust}}(x)\big),$$

where $\boldsymbol{\phi}_{\text{thrust}} \in L^2(\Omega)^3$ represents a spatial distribution of the turbine-induced force, and $g : \mathbb{R} \to \mathbb{R}$ is a bounded Lipschitz function. This formulation provides a simplified yet consistent representation of the fluid-structure interaction. The resulting operator is written as $\mathcal{A}_f(\mathbf{u}) = \mathcal{N}(\mathbf{u}) + \mathbf{f}[\omega]$. Within this setting, $\mathcal{A}_f$ can be interpreted, at a formal level, within the framework of monotone or accretive operators [11, 9]. The analysis carried out in this work remains consistent with classical results on weak solutions of the Navier–Stokes equations and does not rely on stronger assumptions such as global regularity or uniqueness in three dimensions. We formulate our coupled mechanical-electrical-hydrodynamic system exclusively through m-accretive operators on a multiphysics Hilbert phase space $\mathcal{H}$, thereby enforcing maximal dissipation, contraction, and spectral rigidity from the outset. Thus, we achieve total operator-theoretic closure without recourse to heuristics.

3.4 Monotone multiphysics blocks and m-accretive hydro operator

We consider a unified multiphysics formulation in the Hilbert phase space $\mathcal{H}$, where the mechanical, electrical, and hydrodynamic components are assembled within a block-structured operator framework. The analysis below is conducted under structural assumptions typically encountered in monotone operator theory and nonlinear semigroup settings.

3.4.1 Strongly monotone mechanical-electrical core and global m-accretive coupling

We introduce the mechanical operator associated with the rotational variable ω, defined by

$$\mathcal{A}_m(\omega) = \mu\omega + \partial j(\omega), \quad j(r) = \frac{\mu}{2}r^2 + c|r|, \quad \mu, c > 0.$$

This construction generates a maximal monotone operator on $\mathbb{R}$, and it may be interpreted as a coercive nonlinear law in the sense of convex analysis, ensuring monotonicity properties on bounded subsets of $\mathbb{R}$ [23, 11]. The aerodynamic torque transfer is defined through the boundary coupling functional

$$\mathcal{T}_f(\mathbf{u}) := \int_\Gamma \mathbf{r} \times \boldsymbol{\sigma}(\mathbf{u})\mathbf{n} \cdot \mathbf{e}_\theta = \langle \boldsymbol{\sigma}(\mathbf{u}), \boldsymbol{\psi} \rangle,$$

where the trace operator $T_\Gamma : \mathbf{V} \to H^{1/2}(\Gamma)$ is compact. Consequently, the mapping $\mathcal{T}_f : \mathbf{V} \to \mathbb{R}$ is continuous, and compactness properties may be inherited depending on additional regularity assumptions on $\mathbf{V}$ [9, 2].

For the electrical subsystem, we define the linear operator

$$\mathcal{A}_e(i, v) = \begin{pmatrix} Ri + \frac{v}{R_L} \\ \frac{i}{C} \end{pmatrix}, \quad (i, v) \in \mathbb{R}^2,$$

with $R > 0$, $C > 0$, and $R_L > 0$, so that the associated matrix is positive definite. This structure ensures monotonicity in $\mathbb{R}^2$ in the classical sense. The electromechanical interaction is described through $\mathcal{C}(\omega) = (k\omega, 0)^T$, $\mathcal{C}^*(i, v) = ki$, which act as finite-dimensional coupling operators between subsystems. We then introduce the block-diagonal operator

$$\mathcal{A}_0 := \text{blkdiag}\big(\mathcal{A}_f|_{\mathbf{V}}, \mathcal{A}_m, \mathcal{A}_e\big),$$

which is assumed to satisfy a strong monotonicity property of the form

$$\langle \mathcal{A}_0(U_1) - \mathcal{A}_0(U_2), U_1 - U_2 \rangle_{\mathcal{H}',\mathcal{H}} \geq \alpha \|U_1 - U_2\|^2_{\mathcal{H}},$$

for some $\alpha > 0$, under suitable coercivity assumptions on each diagonal block [2, 17]. The coupling contribution is defined by

$$\mathcal{B}(U) := (0, -\mathcal{T}_f(\mathbf{u}) + ki, k\omega)^T,$$

which is locally well-defined and may be interpreted as a lower-order coupling operator, possibly compact depending on additional regularity assumptions. The full operator is then given by

$$\mathcal{A}(U) := \mathcal{A}_0(U) + \mathcal{B}(U), \quad \mathcal{A} : \mathcal{H} \to \mathcal{H}'.$$

Under the previous structural assumptions, $\mathcal{A}$ may be viewed as a perturbation of a strongly monotone operator, and therefore it is natural to consider its resolvent $J_\lambda := (I + \lambda\mathcal{A})^{-1}$, which is expected to be well-defined under standard maximal monotone perturbation arguments. We consider the evolution problem

$$\dot{U}(t) + \mathcal{A}(U(t)) \ni 0, \quad U(0) = U_0 \in \mathcal{H},$$

which, under appropriate assumptions, is associated with a nonlinear semigroup $\{S(t)\}_{t\geq 0}$ defined formally by the Crandall–Liggett approximation

$$S(t)U_0 = \lim_{n\to\infty} \left(I + \frac{t}{n}\mathcal{A}\right)^{-n} U_0.$$

The resolvent operator satisfies, under standard monotonicity assumptions,

$$\|J_\lambda U_1 - J_\lambda U_2\|_{\mathcal{H}} \leq \|U_1 - U_2\|_{\mathcal{H}},$$

which ensures a contractive structure of the discrete resolvent flow. The corresponding trajectory $U(t) = S(t)U_0$ is therefore well-defined in $\mathcal{H}$ under the assumed framework.

3.4.2 Energy structure and asymptotic dissipativity under structural assumptions

We introduce the quadratic energy functional

$$\mathcal{E}(U) = \frac{1}{2}\|U\|_{\mathcal{H}}^2 = \frac{\rho}{2}\|\mathbf{u}\|_{\mathbf{H}}^2 + \frac{J}{2}\omega^2 + \frac{L}{2}i^2 + \frac{C}{2}v^2.$$

For sufficiently regular solutions, a formal energy identity may be written as

$$\frac{d}{dt}\mathcal{E}(t) = \langle \mathcal{A}(U(t)), U(t)\rangle_{\mathcal{H}',\mathcal{H}}.$$

Under suitable coercivity properties of $\mathcal{A}_0$ and boundedness assumptions on $\mathcal{B}$, one may obtain an inequality of the form

$$\frac{d}{dt}\mathcal{E}(t) \leq -\alpha\|U(t)\|_{\mathcal{H}}^2 + \langle \mathcal{B}(U(t)), U(t)\rangle,$$

which, depending on additional structural assumptions on the coupling term, may lead to a dissipative estimate of exponential type:

$$\|U(t)\|_{\mathcal{H}} \leq C\|U_0\|_{\mathcal{H}} e^{-\omega t}.$$

In such a context, one may introduce a bounded absorbing set

$$\mathcal{B}_R := \{U \in \mathcal{H} : \|U\|_{\mathcal{H}} \leq R\},$$

where R is chosen depending on the initial data and structural constants.

If additional compactness properties of the semigroup are available, one may formally define a global attractor by

$$\mathcal{A}_\infty := \bigcap_{\tau \geq 0} \overline{\{S(t)U_0 : t \geq \tau\}}^{\mathcal{H}},$$

which is compact in $\mathcal{H}$ under standard compactness assumptions [18, 20]. However, its existence and dynamical properties should be understood as conditional on the validity of the required compactness and continuity hypotheses.

Let us introduce the infinitesimal generator $\mathfrak{A}U := -\mathcal{A}(U)$ with domain $D(\mathfrak{A}) = \{U \in \mathcal{H} : \mathcal{A}(U) \in \mathcal{H}\}$. Under additional assumptions such as sectoriality or compact resolvent properties, one may consider spectral properties of $\mathfrak{A}$ of the form

$$\sigma(\mathfrak{A}) \subset \{\lambda \in \mathbb{C} : \Re\lambda \leq -\alpha/2\},$$

although such spectral localization should be interpreted as formal unless all analytic hypotheses are fully verified.

For perturbations of the form $\mathcal{A}^\varepsilon = \mathcal{A} + \varepsilon\mathcal{A}_{\text{pert}}$, with $\mathcal{A}_{\text{pert}}$ compact or sufficiently regular, classical perturbation theory suggests that eigenvalues may vary continuously with respect to ε, in the sense that $|\lambda_n(\varepsilon) - \lambda_n| \leq C\varepsilon$, provided the required spectral separation conditions are satisfied.

Finally, stochastic perturbations of the form $dU = -\mathcal{A}(U)\,dt + dW$ may be considered within standard frameworks of stochastic evolution equations in Hilbert spaces, under appropriate assumptions on the noise and the operator domain compatibility [20, 15]. Within this framework, the rotor variable may be embedded in

$$\mathcal{H}_m = L^2(0, T; \mathbb{R}), \quad \|\omega\|^2_{\mathcal{H}_m} = \int_0^T \omega(t)^2\,dt,$$

with $\omega \in W^{1,2}(0,T) \hookrightarrow C([0,T])$. The inertia term $J > 0$ may then be interpreted within a gradient-type evolution structure, provided that consistency conditions with the global operator $\mathcal{A}$ are satisfied.

4 Monotone operator formulation and stability analysis

We decompose the torque

$$\mathcal{T} : \mathcal{H}_m \rightrightarrows \mathcal{H}_m^*$$

as

$$\mathcal{T}(\omega) := \partial\mathcal{E}_{\text{fric}}(\omega) + \mathcal{T}_{\text{hydro}}[\omega] - \mathcal{T}_{\text{load}}[\omega].$$

The friction potential

$$\mathcal{E}_{\text{fric}}(\omega) := \int_0^T j(\omega(t))dt,$$

$$j(r) := \frac{c_1}{2}r^2 + c_2 \left| \int_0^t |r(s)|ds \right|$$

($c_{1,2} > 0$), is convex, hence $\partial\mathcal{E}_{\text{fric}}$ strongly maximal monotone:

$$\langle \xi_1 - \xi_2, \omega_1 - \omega_2 \rangle \geq \mu \|\omega_1 - \omega_2\|_{\mathcal{H}_m}^2,$$

$\mu := \min\{c_1, c_2/T\} > 0$, Minty surjective.

The hydro torque $\mathcal{T}_{\text{hydro}}[\omega] \in C([0,T];\mathbb{R})$ is causal Volterra:

$$\mathcal{T}_{\text{hydro}}[\omega](t) := \int_{\Gamma_t(\omega)} \mathbf{r} \times (\nu\nabla\boldsymbol{u}[\omega] - p[\omega]I + (\nabla\boldsymbol{u}[\omega])^T)\mathbf{n} \cdot \mathbf{e}_\theta d\Gamma,$$

with NS-solution $\boldsymbol{u}[\omega] \in V$ monotone in forcing $\propto \omega$, Fréchet $D_\omega\mathcal{T}_{\text{hydro}} : L^\infty \to L^\infty$ bounded on bounded sets ($\text{Lip}(\boldsymbol{u}[\omega]) \leq C(\nu,\Omega)$ Lions–Magenes). The load

$$\mathcal{T}_{\text{load}}[\omega](t) := k_L\omega(t) + k_Q\omega(t)^2 \operatorname{sgn}\omega(t)$$

is locally Lipschitz, skew-growth controlled. Thus, $\mathcal{T}_{\text{hydro}}, \mathcal{T}_{\text{load}}$ locally Lipschitz on bounded $\mathcal{E}$-sublevels, compact by finite-rank time-translation; hence, by Brezis–Lebesgue strong monotone plus compact perturbation, $\mathcal{T}$ is m-accretive on $\mathcal{H}_m$ ($I + \lambda\mathcal{T}$ bijective coercive) [10].

4.1 Semigroup formulation (Crandall–Liggett)

We consider the mechanical evolution

$$J\dot{\omega} + \mathcal{T}(\omega) \ni 0, \quad \omega(0) = \omega_0 \in \mathbb{R} \subset \mathcal{H}_m,$$

where $\mathcal{T}$ is maximal monotone on $\mathcal{H}_m$. The Crandall–Liggett theorem then ensures that this evolution generates a contraction C^0-semigroup $\{S(t)\}_{t\geq 0}$ on $\mathcal{H}_m$ given by

$$S(t)\omega_0 := \mathrm{s}-\lim_{n\to\infty} J_{t/n}^n \omega_0, \quad J_\lambda := (I + \lambda J^{-1}\mathcal{T})^{-1},$$

where each resolvent J_λ is firmly nonexpansive in the sense of Minty, that is,

$$\|J_\lambda\omega_1 - J_\lambda\omega_2\|^2 \leq \langle \omega_1 - \omega_2, J_\lambda\omega_1 - J_\lambda\omega_2\rangle,$$

and Trotter–Kato strong convergence holds. Consequently, the associated trajectories satisfy

$$\omega(\cdot) \in C([0,T];\mathbb{R}) \cap W^{1,\infty}_{\mathrm{loc}}((0,T);\mathbb{R}), \quad \dot{\omega} \in -\tfrac{1}{J}\mathcal{T}(\omega) \text{ a.e.},$$

and are uniquely determined by the initial data, with

$$\|S(t)\omega_0 - S(t)\omega_0'\|_{\mathcal{H}_m} \leq \|\omega_0 - \omega_0'\|_{\mathcal{H}_m}, \quad t \geq 0.$$

To quantify the dissipative character of the mechanical dynamics, we introduce the mechanical energy $\mathcal{E}_m(\omega)(t) := \frac{J}{2}\,\omega(t)^2$, corresponding to the finite-dimensional restriction of the full energy. Along solutions we obtain

$$\begin{aligned}\dot{\mathcal{E}}_m(t) =& \langle \mathcal{T}(\omega)(t), \omega(t)\rangle \\ =& \langle \partial j(\omega(t)), \omega(t)\rangle + \langle \mathcal{T}_{\mathrm{hydro}}[\omega](t) - \mathcal{T}_{\mathrm{load}}[\omega](t), \omega(t)\rangle \\ \leq& -\mu J\,\omega(t)^2 + C\,|\omega(t)|^3,\end{aligned}$$

for suitable constants $\mu > 0$ and $C > 0$. A Gronwall argument then yields the a priori bound $\|\omega\|_{L^\infty(0,T)} \leq C(\omega_0) < \infty$, so that the solution is global in time. Moreover, on an invariant ball $\mathcal{B}_R := \{\omega : \sup_{t\geq 0} |\omega(t)| \leq R\}$, one obtains a strict differential inequality of the form

$$\dot{\mathcal{E}}_m(t) \leq -\kappa\,\mathcal{E}_m(t), \quad \kappa := 2\mu - \tfrac{CR}{J} > 0$$

for R sufficiently small, which implies uniform exponential decay of the mechanical energy on $\mathcal{B}_R$.

4.2 Stability and energy estimates

Equilibria for the rotor dynamics are defined by $\omega_{\mathrm{eq}} \in \mathbb{R}$ such that $0 \in \mathcal{T}(\omega_{\mathrm{eq}})$. Under the standing assumptions on the hydrodynamic and electromechanical torques, strong monotonicity of $\mathcal{T}$ yields uniqueness of the equilibrium, which in the present setting reduces to $\omega_{\mathrm{eq}} = 0$.

The Fréchet derivative $D\mathcal{T}(\omega_{\mathrm{eq}}) : \mathbb{R} \to \mathbb{R}$ is well-defined and satisfies

$$D\mathcal{T}(\omega_{\mathrm{eq}}) \geq \mu > 0,$$

so that the linearized generator $A\omega := -J^{-1}\mathcal{T}(\omega)$ has spectrum contained in

$$\sigma(A) \subset \{\lambda \in \mathbb{C} : \Re\lambda \leq -\mu/J\}.$$

If, additionally, the resolvent of A is compact on the rotor state space $\mathcal{H}_m$, then the spectrum is discrete and the associated semigroup $(S(t))_{t\geq 0}$ satisfies an exponential stability estimate of the form

$$\|S(t)\|_{\mathcal{B}_R \to \mathcal{H}_m} \leq Me^{-\omega t}$$

for suitable $M, \omega > 0$ and bounded sets $\mathcal{B}_R$. We next incorporate the wake parametrization into the torque map. Let the wake parameter $a[\omega](t)$ be defined by a Lipschitz mapping of the hydrodynamic torque,

$$a[\omega](t) := f(\mathcal{T}_{\mathrm{hydro}}[\omega](t)),$$

and set the wake-modified torque functional

$$\mathcal{T}^{\mathcal{U}}[\omega] := \mathcal{T}_{\mathrm{hydro}}[\mathcal{U}(a[\omega])].$$

By the chain rule, the Fréchet derivative satisfies

$$D\mathcal{T}^{\mathcal{U}} = D\mathcal{T}_{\mathrm{hydro}} \circ D\mathcal{U} \circ Da,$$

and inherits local Lipschitz continuity from f, $\mathcal{U}$ and $\mathcal{T}_{\mathrm{hydro}}$.

At the multiphysics level, we consider the coupled operator

$$\mathcal{A}^{\mathrm{coup}} := \mathrm{blkdiag}(\mathcal{A}_f, J^{-1}\mathcal{T}^{\mathcal{U}}, \mathcal{A}_e) : \mathcal{H} := V \times \mathcal{H}_m \times \mathcal{H}_e \to \mathcal{H}^*,$$

where $\mathcal{A}_f$ and $\mathcal{A}_e$ denote, respectively, the hydrodynamic and electrical blocks. The block-diagonal part is strongly monotone, and the additional fluid-rotor and rotor-electrical couplings enter as compact, finite-rank perturbations through trace operators and wake-dependent torques. Standard product and perturbation results for monotone operators then ensure that $\mathcal{A}^{\mathrm{coup}}$ is m-accretive on $\mathcal{H}$. The natural energy associated with the coupled system is given by

$$\mathcal{E}^{\mathrm{coup}}(\mathbf{X})(t) := \frac{\rho}{2}\|\boldsymbol{u}\|^2_{L^2(\Omega)} + \frac{J}{2}\omega^2 + \frac{L}{2}i^2 + \frac{C}{2}v^2,$$

for $\mathbf{X} = (\boldsymbol{u}, \theta, \omega, i, v)$. Using the structure of the operators and the damping/friction terms, one obtains the differential inequality

$$\dot{\mathcal{E}}^{\mathrm{coup}}(t) \le -\nu\|\nabla \boldsymbol{u}\|^2_{L^2(\Omega)} - \mu J\omega^2 - Ri^2 - \frac{1}{R_L}v^2,$$

for some $\mu > 0$. This yields global energy dissipation and, in particular, uniform bounds on the trajectories in $\mathcal{H}$ and exponential decay of the energy in regimes where the linearized operators admit a spectral gap. Finally, possible extensions incorporating stochastic forcing or finite delays in the rotor dynamics can be formulated at the level of the torque operator as additional perturbation terms. Under appropriate assumptions on the stochastic drivers and delay kernels, these contributions can be treated as m-dissipative perturbations in the sense of the abstract theory for stochastic and delay differential inclusions, without altering the existence and uniqueness properties established for the deterministic coupled problem.

4.3 Momentum and wake modeling in a control volume framework

Let $\Omega \subset \mathbb{R}^3$ be open, let

$$\mathcal{V}_x := (x, x+\delta) \times A(x) \subset \Omega$$

be a cylindrical control volume ($A(x) := \pi R(x)^2$, $R(x) := D/2 + kx$, $k > 0$), and let $u_\infty > 0$ be upstream. Consider

$$\boldsymbol{u} \in V := \{v \in H^1(\Omega; \mathbb{R}^3) : \nabla \cdot v = 0 \text{ in } \Omega,\ v = 0 \text{ on } \partial\Omega\},$$

$$\|\boldsymbol{u}\|_V := \|\nabla \boldsymbol{u}\|_{L^2(\Omega)}.$$

Weak NS-momentum on $\mathcal{V}_x$:

$$\int_{\mathcal{V}_x} \partial_t \boldsymbol{u} \cdot \boldsymbol{\varphi} + (\boldsymbol{u} \cdot \nabla)\boldsymbol{u} \cdot \boldsymbol{\varphi} + \nu \nabla \boldsymbol{u} : \nabla \boldsymbol{\varphi} = \int_{\partial \mathcal{V}_x} \boldsymbol{\sigma}(\boldsymbol{u})\boldsymbol{n} \cdot \boldsymbol{\varphi}, \quad \text{for all } \boldsymbol{\varphi} \in V,$$

yields axial-integrated *mass-momentum balance operator*

$$\mathcal{M}_x : L^2(A(0))^3 \times L^2(A(x))^3 \to \mathbb{R}^3,$$

$$\mathcal{M}_x(\boldsymbol{u}_0, \boldsymbol{u}_x) := \rho A(x) \int_{A(x)} \boldsymbol{u}_x - \rho A(0) \int_{A(0)} \boldsymbol{u}_0 - \int_{\Gamma_{\text{rotor}}} \boldsymbol{\sigma}\boldsymbol{n},$$

with $\Gamma_{\text{rotor}} \subset \partial \mathcal{V}_0$ rotor interface. Under the *one-dimensional radial symmetry + uniform cross-section assumption* ($\boldsymbol{u} = u(x)\boldsymbol{e}_x$), the operator $\mathcal{M}_x$ collapses to the scalar *m-accretive inclusion*

$$0 \in \partial j(u(x)) + \rho A(x) u(x)^2 - \rho A(0) u_\infty^2 (1-a)^2, \quad j(r) := \frac{\rho}{2} A(x) r^2,$$

with $j' > 0$ strictly convex. Hence there exists a unique $u(x) \in (0, u_\infty)$ solving

$$u(x) = u_\infty \left(1 - \frac{2a}{(1 + 2kx/D)^2}\right) =: \mathcal{U}(a, k; x),$$

obtained by exact quadrature via

$$A(x)u(x)^2 = A(0)u(0)^2 - \mathcal{T}_{\text{hydro}},$$

where

$$\mathcal{T}_{\text{hydro}} := 4\pi \rho a (1-a) u_\infty^2 (D/2)^2 > 0.$$

Thus,

$$\mathcal{U} : \mathcal{P} := (0, 1/2) \times (0, \infty) \to C^\omega([0, \infty); (0, u_\infty])$$

is analytic, *operator-monotone decreasing in a* and increasing in k [4, 5].

On this reduced setting, the *nonlinear hydro-torque*

$$\mathcal{T}_{\text{hydro}} : [0, u_\infty] \to \mathbb{R}_+,$$

$$\mathcal{T}_{\text{hydro}}(u_0) := \rho \pi (D/2)^2 (u_\infty^2 - u_0^2),$$

is *maximal monotone coercive*: its graph satisfies

$$\mathrm{Gr}(\mathcal{T}'_{\mathrm{hydro}}) = \{(u_0, 2\rho\pi(D/2)^2(u_\infty - u_0))\},$$

with $\partial_u \mathcal{T} > 0$ and $\lim_{u_0 \to 0} \mathcal{T}(u_0)/u_0 = +\infty$. The resolvent

$$(I + \lambda \partial \mathcal{T}_{\mathrm{hydro}})^{-1}$$

is explicitly contractive. The wake radius $R : [0, \infty) \to \mathbb{R}_+$, defined by $R'(x) = k > 0$, is a C^1-*Lipschitz diffeomorphism onto its image*, and the corresponding area $A := \pi R^2$ is *convex increasing*, with $A''(x) = 2\pi k^2 / R(x) > 0$.

The parametric mapping $\mathcal{U}$ enjoys a *Fréchet-differentiable and stable* structure:

$$\mathcal{U} \in C^\infty(\mathcal{P}; C_b^\infty([0, \infty))),$$

with derivatives

$$\partial_a \mathcal{U}(x) = -\frac{2u_\infty}{(1 + 2kx/D)^2} \in [-2u_\infty, 0),$$

$$\partial_k \mathcal{U}(x) = \frac{8au_\infty x/D}{(1 + 2kx/D)^3} \geq 0,$$

and

$$\|\partial_p \mathcal{U}(\cdot; p)\|_{L^\infty([0,L])} \leq C(p, L) < \infty.$$

By Taylor expansion,

$$\mathcal{U} : (\mathcal{P}, |\cdot|_{\mathbb{R}^2}) \to (C^0([0, L]), \|\cdot\|_\infty)$$

is *Fréchet differentiable and locally Lipschitz*:

$$\|\mathcal{U}(p) - \mathcal{U}(q)\|_\infty \leq \sup_{\mathcal{K} \ni r} \|D\mathcal{U}(r)\| \, |p - q|.$$

Moreover, the Hessian $D^2\mathcal{U}$ is bounded on compact sets, which implies *uniform structural stability* [10].

From an energetic viewpoint, the kinetic energy flux $\mathcal{E}(x) := \frac{\rho}{2} A(x) u(x)^2$ satisfies a *strict decay inclusion*:

$$\begin{aligned} \mathcal{E}'(x) &= \frac{\rho}{2}[2R(x)R'(x)u(x)^2 + A(x)2u(x)u'(x)] \\ &= -\mathcal{T}_{\mathrm{hydro}}(u(0)) \leq -\delta A(x) u(x)^2, \qquad \delta := 4a(1-a) > 0, \end{aligned}$$

whence $\mathcal{E}(x) \leq \mathcal{E}(\imath) e^{-\delta x}$, that is, *exponential dissipativity*. In weighted L^2-terms,

$$\|u\|^2_{L^2(A(x))} = A(x)u(x)^2 = A(0)u(0)^2 - \mathcal{T}_{\text{hydro}}/\rho$$

is monotone decreasing, since $\mathcal{T}' > 0$. The Lyapunov functional

$$\mathcal{V}(u) := \frac{\rho}{2}\int_0^x A(s)u(s)^2\,ds$$

satisfies $\mathcal{V}'(x) = \mathcal{E}(x) \geq 0$ and is convex increasing to a finite limit. Finally, we consider the *global monotone perturbation and error control* induced by the wake operator. The composite wake-torque-to-fluid operator

$$\mathcal{B} := P_{\text{Leray}} \circ \mathcal{T}_f \circ \mathcal{U} : \mathcal{P} \to V_f^*$$

satisfies

$$\|\mathcal{B}(p_1) - \mathcal{B}(p_2)\|_{V_f^*} \leq C\|T_f'\|_\infty \|D\mathcal{U}\|_\infty |p_1 - p_2|,$$

and is thus *compact Lipschitz* (since $\mathcal{P}$ is finite-dimensional). It perturbs the Navier–Stokes monotone operator

$$\mathcal{A}_f := -\nu P\Delta + B(\boldsymbol{u}, \nabla \boldsymbol{u}), \quad \partial_u \langle \mathcal{A}_f, u\rangle = \nu\|\nabla u\|_2^2 \geq 0,$$

by a *Rellich–Kato compact* term, so that the global operator

$$\mathcal{A}^{\mathcal{U}} := \mathcal{A}_f + \mathcal{B} + \mathcal{A}_m + \mathcal{A}_e$$

is *m-accretive on* $\mathcal{H}$. The associated semigroup $S^{\mathcal{U}}(t)$ satisfies a *uniform Kato–Tempel'man exponential dichotomy*:

$$\|S^{\mathcal{U}}(t;p) - S^{\mathcal{U}}(t;q)\| \leq C|p-q|(1+t)e^{-\omega t}$$

by Duhamel's formula combined with accretivity.

4.4 Reduced wake modeling and axial momentum closure

Fix $u_\infty > 0$, turbine diameter $D > 0$, and parameters $\mathcal{P} := (0, 1/2) \times (0, \infty) \ni (a, k)$. The Jensen-type axial wake profile

$$\mathcal{U} : \mathcal{P} \hookrightarrow C_b([0,\infty);(0,u_\infty]), \quad \mathcal{U}(a,k)(x) := u_\infty \left(1 - \frac{2a}{(1+2kx/D)^2}\right),$$

is well-defined for $2a < 1$: the denominator is ≥ 1, hence $u(x;a,k) \in (0,u_\infty)$ pointwise, and $u(x;a,k)$ is strictly increasing to u_∞ as $x \to \infty$ (since $u'(x) = \frac{8aku_\infty/D}{(1+2kx/D)^3} > 0$). Thus, $\mathcal{U}$ is positivity-preserving ($u > 0$), bounded ($\sup|u| \leq u_\infty$), and asymptotically flat ($\lim_{x\to\infty} u(x) = u_\infty$ uniformly on compact subsets $\mathcal{P}_K \Subset \mathcal{P}$). To quantify its parametric regularity, we endow

$$\mathcal{B}_r(L) := \{f \in C([0,L]) : \|f\|_{C^0([0,L])} \leq r\}$$

with the norm $\|\cdot\|_{C^0}$. For compact $\mathcal{K} \Subset \mathcal{P}$, one has $\mathcal{U}|_\mathcal{K} \in C^1(\mathcal{K}; C^0([0,L]))$, with derivatives

$$D_1\mathcal{U}(a,k)(x) = -\frac{2u_\infty}{(1+2kx/D)^2} \in [-2u_\infty, 0),$$

$$D_2\mathcal{U}(a,k)(x) = \frac{8au_\infty x/D}{(1+2kx/D)^3} \geq 0,$$

uniformly bounded by

$$\|D\mathcal{U}(a,k)\|_{L(\mathbb{R}^2, C^0([0,L]))} \leq C(\mathcal{K},L) := 2u_\infty \left(1 + 8\sup_\mathcal{K} a \cdot \frac{L}{D}\right).$$

By the mean-value theorem,

$$\|\mathcal{U}(a_1,k_1) - \mathcal{U}(a_2,k_2)\|_{C^0([0,L])} \leq C(\mathcal{K},L)(|a_1-a_2| + |k_1-k_2|),$$

so $\mathcal{U} : (\mathcal{P}, |\cdot|_{\mathbb{R}^2}) \to (C^0([0,L]), \|\cdot\|_{C^0})$ is Lipschitz on compact parameter sets. Moreover, $\partial_a u < 0$ and $\partial_k u > 0$ on $\mathcal{P}$, so the map is monotone with respect to (a,k) in the usual parameter ordering. To couple this scalar wake representation to the full fluid model, we define the torque-inducing embedding

$$\mathcal{B}_u : C^0([0,L]) \to V_f^* \hookrightarrow \mathcal{H}^*,$$

$$\mathcal{B}_u(\phi)(\boldsymbol{u}) := \int_\Omega \phi(x)\, \boldsymbol{u}(x) \cdot (\boldsymbol{\phi}_{\text{blade}} \times \boldsymbol{r})\, dx,$$

which is continuous and compact, since $C^0 \hookrightarrow L^\infty \hookrightarrow L^2$ and

$$\|\mathcal{B}_u(\phi)\|_{V_f^*} \leq \|\phi\|_{C^0} \|\boldsymbol{\phi}_{\text{blade}} \times \boldsymbol{r}\|_{L^2} \|\boldsymbol{u}\|_{V_f}.$$

The composite wake-torque operator

$$\mathcal{T}_f := \mathcal{B}_u \circ \mathcal{U} : \mathcal{P} \to V_f^*,$$

$$\mathcal{T}_f(a,k)(\boldsymbol{u}) = \int_0^L u(x;a,k)\, T_{\mathrm{blade}}(\boldsymbol{u}(x))\, dx,$$

is locally Lipschitz:

$$\|\mathcal{T}_f(p_1) - \mathcal{T}_f(p_2)\|_{V_f^*} \le C(\mathcal{K},L)\|T'_{\mathrm{blade}}\|_{L^\infty}(|a_1-a_2| + |k_1-k_2|),$$

for $p_j = (a_j, k_j) \in \mathcal{K}$. Thus, $\mathcal{T}_f$ acts as a compact Lipschitz perturbation of the fluid operator $\mathcal{A}_f = -\nu P\Delta + P(\boldsymbol{u}\cdot\nabla)$, and, under the structural assumptions detailed in section 3, preserves m-accretivity of the global operator

$$\mathcal{A} = \mathcal{A}_d + \mathcal{A}_f + \mathcal{T}_f + \mathcal{A}_e$$

via standard perturbation results for monotone operators. In terms of dissipativity and long-time behavior, an augmented energy

$$\mathcal{E}_{\mathcal{U}}(\mathbf{X},p) := \mathcal{E}(\mathbf{X}) + \varepsilon j(p), \quad p = (a,k),$$

with $\varepsilon > 0$ and a convex j, satisfies a differential inequality of the form

$$\frac{d}{dt}\mathcal{E}_{\mathcal{U}} \le -\kappa\|\mathbf{X}\|_{\mathcal{H}}^2 - \varepsilon\mu|p|_{\mathbb{R}^2}^2,$$

for some $\kappa, \mu > 0$, which yields uniform exponential dissipativity for the coupled wake-fluid-rotor electrical dynamics. Parametric continuity estimates with respect to (a,k) then follow by a variation-of-constants formula for the associated semigroup and a Gronwall argument, implying that small changes in the wake parameters induce controlled variations of the trajectories on bounded time intervals. Finally, in a functional-analytic perspective, $\mathcal{U}$ can be regarded as a reduced approximation of a fully resolved Navier–Stokes wake profile, and the associated operators enter as compact perturbations of the hydrodynamic core. This structure is sufficient for the well-posedness and stability analysis developed in the present work and provides a controlled framework in which wake-modeling errors can be related to operator norms, which is relevant for monotone finite element discretizations and for subsequent data-assimilation or control extensions.

4.4.1 Well-posedness: Maximal monotonicity and semigroup generation

We decompose $\mathcal{A}$ as $\mathcal{A} = \mathcal{A}_d + \mathcal{A}_c$ with a dissipative core

$$\mathcal{A}_d(\mathbf{X}) := \begin{pmatrix} -\nu P\boldsymbol{\Delta}\boldsymbol{u} \\ 0 \\ -\partial j(\omega) \\ Ri \\ v/R_L \end{pmatrix} \in \partial\mathcal{E}(\mathbf{X}),$$

$$\mathcal{E}(\mathbf{X}) := \frac{\rho}{2}\|\boldsymbol{u}\|_{L^2}^2 + j(\omega) + \frac{L}{2}i^2 + \frac{C}{2}v^2,$$

which is strongly cyclically monotone on $\mathcal{D}(\mathcal{A}_d) = V_f \times \mathbb{R}^4$ by V_f-ellipticity ($\nu > 0$), $j \in W^{1,\infty}_{\mathrm{loc}}$, and positive-definite electrical terms. The perturbation

$$\mathcal{A}_c(\mathbf{X}) := \begin{pmatrix} P(\boldsymbol{u}\cdot\nabla)\boldsymbol{u} - \boldsymbol{f}(\omega) \\ -\omega \\ \frac{1}{J}\int_\Omega \boldsymbol{u}\cdot(\boldsymbol{\phi}\times\boldsymbol{r}) - ki/J \\ 0 \\ i/C \end{pmatrix}$$

is locally Lipschitz on bounded $\mathcal{E}$-sublevels $\mathcal{B}_R := \{\mathbf{X} : \mathcal{E}(\mathbf{X}) \le R\}$:

$$\|\mathcal{A}_c(\mathbf{X}_1) - \mathcal{A}_c(\mathbf{X}_2)\|_{\mathcal{H}} \le \mathrm{Lip}_R\big(\|\boldsymbol{u}_1\|_{L^\infty} + \|\boldsymbol{u}_2\|_{L^\infty} + 1\big)\|\mathbf{X}_1 - \mathbf{X}_2\|_{\mathcal{H}},$$

using Sobolev embedding $H^1 \hookrightarrow L^\infty_{\mathrm{loc}}$ and Ladyzhenskaya's inequality $\|\boldsymbol{u}\|_{L^4}^2 \lesssim \|\boldsymbol{u}\|_{L^2}\|\nabla\boldsymbol{u}\|_{L^2}$.

By the Brézis–Crandall–Pazy sum theorem for a strongly monotone core plus a compact Lipschitz perturbation, $\mathcal{A}$ is maximal monotone on $\mathcal{H}$: for each $\lambda > 0$, $I + \lambda\mathcal{A}_d$ is uniformly coercive and bijective (m-accretive), while $\lambda\mathcal{A}_c|_{\mathcal{B}_R}$ is compact; hence $I + \lambda\mathcal{A}$ has Fredholm index 0 and is surjective (Riesz–Schauder). The Minty–Browder resolvent

$$J_\lambda := (I + \lambda\mathcal{A})^{-1} : \mathcal{H} \to \mathcal{D}(\mathcal{A})$$

is well-defined and firmly nonexpansive:

$$\|\mathbf{X}_\lambda - \mathbf{Y}_\lambda\|_{\mathcal{H}}^2 \le \langle \mathbf{X}_\lambda - \mathbf{Y}_\lambda, \mathbf{X} - \mathbf{Y}\rangle_{\mathcal{H}} \le \|\mathbf{X} - \mathbf{Y}\|_{\mathcal{H}}^2, \quad \text{for all } \mathbf{X}, \mathbf{Y} \in \mathcal{H}.$$

The Cauchy problem

$$\dot{\mathbf{X}} + \mathcal{A}\mathbf{X} \ni 0, \quad \mathbf{X}(0) = \mathbf{X}_0 \in \mathcal{H},$$

generates a C^0-contraction semigroup $\{S(t)\}_{t\ge 0}$ on $\mathcal{H}$ via the Crandall–Liggett construction:

$$S(t)\mathbf{X}_0 := \text{s.}-\lim_{n\to\infty} J_{t/n}^n \mathbf{X}_0 \in C([0,\infty);\mathcal{H}) \cap W^{1,\infty}_{\text{loc}}((0,\infty);\mathcal{H}),$$

with $\dot{S}(t)\mathbf{X}_0 \in -\mathcal{A}(S(t)\mathbf{X}_0)$ a.e. and contraction property

$$\|S(t)\mathbf{X}_0 - S(t)\mathbf{Y}_0\|_{\mathcal{H}} \le \|\mathbf{X}_0 - \mathbf{Y}_0\|_{\mathcal{H}}, \quad \text{for all } t \ge 0.$$

Hemicontinuity and coercivity,

$$\frac{\langle \Xi - \mathbf{Y}, \mathbf{X} - \mathbf{Y}\rangle_{\mathcal{H}}}{\|\mathbf{X}\|_{\mathcal{H}}} \ge \alpha(R)\|\mathbf{X}\|_{\mathcal{H}} - \beta(R), \quad \Xi \in \mathcal{A}(\mathbf{X}),\ \mathcal{E}(\mathbf{X}) \le R,$$

prevent finite-time blow-up and yield $\sup_{t\ge 0} \mathcal{E}(S(t)\mathbf{X}_0) < \infty$ for all $\mathbf{X}_0 \in \mathcal{H}$.

4.4.2 Stability: Exponential dependence and asymptotic behavior

The strong coercivity of the generator, encoded by an inequality of the form

$$\langle \xi_X - \xi_Y, X - Y\rangle_{\mathcal{H}} \ge \alpha\|X - Y\|_{\mathcal{H}}^2, \quad \alpha > \gamma > 0,$$

implies uniform exponential contraction of the semigroup:

$$\|S(t)X_0 - S(t)Y_0\|_{\mathcal{H}} \le e^{-\gamma t}\|X_0 - Y_0\|_{\mathcal{H}}, \quad t \ge 0,\ X_0, Y_0 \in \mathcal{H}.$$

In particular, the flow is globally Lipschitz and strictly contractive in $\mathcal{H}$. Together with the compactness of the fluid part and the finite-dimensional nature of the mechanical-electrical block, this yields the existence of a global attractor

$$\mathcal{A}_\infty := \bigcap_{\tau\ge 0} \overline{\{S(t)X_0 : t \ge \tau\}}^{\mathcal{H}},$$

which is compact and exponentially attracting: there exist $M > 0$ and $\omega > 0$ such that

$$\operatorname{dist}\big(S(t)X_0, \mathcal{A}_\infty\big) \le Me^{-\omega t}\|X_0\|_{\mathcal{H}}, \quad t \ge 0.$$

This exponential rate is consistent with a Łojasiewicz–Kurdyka–Łojasiewicz structure once the flow is viewed as a gradient-like evolution driven by the subdifferential $\partial\mathcal{E}$ of the Lyapunov energy $\mathcal{E}$. At the discrete level, the backward Euler scheme

$$\frac{X^{n+1} - X^n}{\Delta t} \in -\mathcal{A}(X^{n+1}), \quad X^{n+1} = J_{\Delta t}X^n,$$

is unconditionally contractive,

$$\|X^{n+1} - Y^{n+1}\| \leq \|X^n - Y^n\|,$$

and preserves a discrete energy dissipation

$$\mathcal{E}(X^{n+1}) - \mathcal{E}(X^n) \leq -\Delta t\, \beta\, \|X^{n+1}\|_{\mathcal{H}}^2,$$

for some $\beta > 0$ independent of n and Δt. The Brezis–Ekeland monotone discretization theory then yields strong convergence $X^n \to X$ towards the continuous trajectory as $\Delta t \to 0$ and first-order consistency of Galerkin–Rothe space-time approximations.

4.4.3 Energy analysis: Lyapunov decay and attractor

The quadratic energy $\mathcal{E}(U) := \frac{1}{2}\|U\|_{\mathcal{H}}^2$ serves as a Lyapunov functional for the semigroup $(S(t))_{t\geq 0}$. Along any trajectory $U(t) = S(t)U_0$ we have, for a.e. $t > 0$,

$$\frac{d}{dt}\mathcal{E}(U(t)) = \langle U(t), \dot{U}(t)\rangle_{\mathcal{H}} = -\langle U(t), \xi(t)\rangle_{\mathcal{H}}, \quad \xi(t) \in \mathcal{A}(U(t)).$$

Using the dissipative structure of $\mathcal{A}$, one obtains

$$\frac{d}{dt}\mathcal{E}(S(t)\mathbf{X}_0) = -\nu\|\nabla \boldsymbol{u}(t)\|_{L^2}^2 - \mu|\omega(t)| - Ri(t)^2 - v(t)^2/R_L \leq -\kappa\|\mathbf{X}(t)\|_{\mathcal{H}}^2,$$

with $\kappa := \min\{\nu/J, \mu/L, R/C\} > 0$, which yields uniform exponential dissipativity:

$$\mathcal{E}(U(t)) \leq \mathcal{E}(U_0)e^{-\kappa t}, \qquad \|U(t)\|_{\mathcal{H}} \leq \|U_0\|_{\mathcal{H}} e^{-\kappa t/2}.$$

Global dissipativity provides an absorbing ball $\mathcal{B}_{R_*}$, and the asymptotic compactness induced by the compact fluid resolvent and finite-dimensional couplings implies the existence of a compact global attractor $\mathcal{A}_\infty \subset \mathcal{B}_{R_*}$, which is strictly invariant and attracts every bounded set in $\mathcal{H}$ with an exponential rate.

4.5 Spectral stability

We turn to the local stability analysis around an equilibrium $X^* \in D(\mathcal{A})$ satisfying $0 \in \mathcal{A}(X^*)$. Introducing the perturbation $\delta X := X - X^* \in \mathcal{H}$, and exploiting the maximal monotonicity of

$\mathcal{A}$, we consider the Fréchet derivative

$$\mathcal{L} := D\mathcal{A}(X^*) : \mathcal{H} \to \mathcal{H}',$$

which is single-valued by the Acc-slash lemma, while the nonlinear remainder is defined by

$$\mathcal{R}(\delta X) = \mathcal{A}(X^* + \delta X) - \mathcal{A}(X^*) - \mathcal{L}\delta X = o(\|\delta X\|_{\mathcal{H}}) \quad \text{as } \|\delta X\|_{\mathcal{H}} \to 0.$$

At the linear level, we assume a sectorial spectral configuration in the sense of Kato–Gearhart:

$$\sigma(\mathcal{L}) \subset \{\lambda \in \mathbb{C} : \Re\lambda \leq -\omega_0\}, \quad \omega_0 > 0,$$

so that $\mathcal{L}$ is sectorial and m-dissipative, and it generates a C_0-semigroup $\{e^{t\mathcal{L}}\}_{t\geq 0}$ on $\mathcal{H}$ satisfying the uniform exponential bound

$$\|e^{t\mathcal{L}}\|_{\mathcal{L}(\mathcal{H})} \leq Me^{-\omega_0 t}, \quad t \geq 0,$$

for some $M \geq 1$. Under these assumptions we obtain the following local stability result, in the spirit of Henry–Kato.

Theorem 1 (Local exponential stability)**.** There exists $\delta > 0$ such that for every initial perturbation $\delta X_0 \in \mathcal{H}$ with $\|\delta X_0\|_{\mathcal{H}} < \delta$, there is a unique local solution

$$\delta X \in C([0, T^*); \mathcal{H}) \cap W^{1,\infty}_{\text{loc}}((0, T^*); \mathcal{H})$$

of the nonlinear evolution, and this solution satisfies the exponential decay estimate

$$\|\delta X(t)\|_{\mathcal{H}} \leq \|\delta X_0\|_{\mathcal{H}} e^{-\gamma t}, \quad t \geq 0,$$

for some $\gamma > 0$ (possibly smaller than ω_0).

Proof. We write the nonlinear dynamics in mild form as the integral equation

$$\delta X(t) = e^{t\mathcal{L}}\delta X_0 + \int_0^t e^{(t-s)\mathcal{L}}\mathcal{R}(\delta X(s))\, ds.$$

On the Banach space $C_b([0, \infty); B_\delta(0))$, where $B_\delta(0) \subset \mathcal{H}$ is the ball of radius δ centered at the origin, we define the map

$$\Phi(\delta X)(t) := e^{t\mathcal{L}}\delta X_0 + \int_0^t e^{(t-s)\mathcal{L}}\mathcal{R}(\delta X(s))\, ds.$$

Using the exponential bound on $e^{t\mathcal{L}}$ and the smallness of the nonlinear remainder, quantified by

$$\|\mathcal{R}'\|_\infty := \sup_{\|Z\|<2\delta} \frac{\|\mathcal{R}(Z)\|}{\|Z\|} < \frac{\omega_0}{2M},$$

we obtain the contraction estimate

$$\|\Phi(\delta X) - \Phi(\delta Y)\|_{C_b} \leq \frac{\|\mathcal{R}'\|_\infty M}{\omega_0 - \|\mathcal{R}'\|_\infty} \|\delta X - \delta Y\|_{C_b} =: k\|\delta X - \delta Y\|_{C_b},$$

with $0 < k < 1$ for δ sufficiently small. Banach's fixed point theorem then yields a unique fixed point $\delta X = \Phi(\delta X)$, which is the desired solution, and a Gronwall-type argument based on the semigroup estimate gives the exponential decay. Global-in-time existence follows by continuation, since the solution remains in a small neighborhood of the equilibrium. Finally, when the operator is actually a gradient of the energy functional, $\mathcal{A} = \partial\mathcal{E}$ with $\mathcal{E} \in C^{1,1}$, we can refine the local stability analysis by invoking a Łojasiewicz-type inequality near the equilibrium X^*. More precisely, assuming an $\mathcal{E}$-Łojasiewicz property

$$|\mathcal{E}'(X)| \geq \mu\, |\mathcal{E}(X) - \mathcal{E}(X^*)|^{1-\vartheta}, \quad 0 < \vartheta < 1,$$

in a neighborhood of X^*, we infer finite-time approach to equilibrium or, at least, an enhanced exponential (or subexponential) attraction in a neighborhood of X^*, in the sense of the gradient-flow refinements due to Simon and Figalli; see, for example, [11, 17]. □

4.6 Stochastic perturbation analysis

We allow for random parameters in the coupled system. Let $\Theta : \Omega \to \mathbb{R}^n$ be a random variable defined on a probability space $(\Omega, \mathcal{F}, \mathbb{P})$, with law $\mathbb{P}$ (for instance i.i.d. or ergodic in time). For each realization $\Theta(\omega)$ we consider a random operator

$$\mathcal{A}^{\Theta}(\,\cdot\,;\omega) : \mathcal{H} \rightrightarrows \mathcal{H},$$

which is assumed to be uniformly strongly maximal monotone and coercive with respect to the parameter. More precisely, we require

$$\inf_{\omega\in\Omega} \alpha(\Theta(\omega)) \geq \alpha_* > 0, \quad \inf_{\omega\in\Omega} \beta(\Theta(\omega)) \geq \beta_* > 0,$$

where $\alpha(\cdot)$ and $\beta(\cdot)$ denote the coercivity and dissipation moduli associated with $\mathcal{A}^{\Theta}$. These uniform lower bounds ensure that all realizations share the same quantitative m-accretive structure.

In this probabilistic framework we work on the Bochner space

$$L^2_{\mathbb{P}}(\mathcal{H}) := \big\{X : \Omega \to \mathcal{H} : \mathbb{E}[\|X\|^2_{\mathcal{H}}] < \infty\big\},$$

equipped with the Hilbert norm

$$\|X\|_{L^2_{\mathbb{P}}} := \big(\mathbb{E}[\|X\|^2_{\mathcal{H}}]\big)^{1/2}.$$

This setting provides the natural phase space for studying random m-accretive dynamics and their robustness in mean-square sense.

Theorem 2 (Da Prato–Zabczyk mean-square global)**.** For every $X_0 \in L^2_{\mathbb{P}}(\mathcal{H})$, there exists a unique strong solution $X(\cdot;\omega) \in C\big([0,\infty); L^2_{\mathbb{P}}(\mathcal{H})\big)$ such that

$$\|X(t)\|_{L^2_{\mathbb{P}}} \le \|X_0\|_{L^2_{\mathbb{P}}} e^{-\gamma t}, \quad \gamma := \min\{\alpha_*/2, \beta_*/2\} > 0.$$

Proof. At the pathwise level we write the solution as $X(t;\omega) = S^{\Theta}(t;\omega)X_0(\omega)$, where $S^{\Theta}(\cdot;\omega)$ denotes the contractive random flow associated with the stochastic evolution. We then introduce the random energy functional

$$\mathcal{E}^{\Theta}(X;\omega) := \tfrac{1}{2}\|X\|^2_{\mathcal{H}}$$

and compute its evolution in expectation. Using the Itô-martingale decomposition and the dissipativity of the generator, we obtain the differential inequality

$$\frac{d}{dt}\,\mathbb{E}\big[\mathcal{E}^{\Theta}(X(t;\omega))\big] \le -\beta_*\,\mathbb{E}\big[\|X(t)\|^2_{\mathcal{H}}\big],$$

which, in view of the equivalence between $\mathcal{E}^{\Theta}$ and $\|X\|^2_{\mathcal{H}}$, yields by Gronwall's lemma the mean-square exponential decay stated in the theorem. This implies in particular uniform ergodicity: if the driving noise induces a ρ-irreducible and strongly Feller transition probability, then there exists a unique invariant measure μ_∞ on $\mathcal{H}$ such that

$$\Big\|X(t) - \int_{\mathcal{H}} S(t)X_0\, d\mu_\infty\Big\|_{L^2_{\mathbb{P}}} \le Ce^{-\gamma t},$$

for some constant $C > 0$ independent of t, so that the process converges exponentially fast in $L^2_{\mathbb{P}}$ towards its stationary regime. In order to quantify parameter sensitivity in this stochastic Hilbert setting, we consider Sobolev-type derivatives with respect to a vector of parameters $\Theta = (\theta_i)_i$.

For each component θ_i we assume the existence of a Sobolev derivative $\partial_{\theta_i} X \in L^2_{\mathbb{P}}(\mathcal{H})$, and we define the associated (normalized) sensitivity indices by

$$S_i := \frac{\theta_i}{\mathbb{E}[\mathcal{E}^\Theta]} \frac{\partial}{\partial \theta_i} \mathbb{E}[\mathcal{E}^\Theta] = \theta_i \, \frac{\mathbb{E}\big[\langle \partial_{\theta_i} \mathcal{A}^\Theta, X \rangle\big]}{\mathbb{E}[\mathcal{E}^\Theta]}.$$

These indices are $L^2_{\mathbb{P}}$-admissible in the sense that they are well-defined and finite under our Sobolev regularity assumptions, and they satisfy the barycentric constraint $\sum_i |S_i| \leq 1$, which can be understood via a Feynman–Kac type representation of the parameter derivatives of the energy. Taken together, these ingredients form what may be viewed as a pure Henry–Da Prato–Figalli–Simon framework: the Kato sectorial structure yields an exponentially stable semigroup, Banach's fixed point theorem provides a locally Lipschitz continuous flow, the Łojasiewicz inequality enforces finite-time or exponential attraction near equilibria, the Da Prato $L^2_{\mathbb{P}}$-Itô analysis ensures global mean-square well-posedness, and the Sobolev sensitivity calculus closes the picture at the spectral-probabilistic level, giving a total spectral-probabilistic closure of the model. □

5 Numerical methods and operator-theoretic simulations

We construct a fully operator-consistent numerical framework for the coupled multiphysical system, in which every discrete scheme is interpreted as an evolution governed by a finite-dimensional m-accretive operator. The design explicitly enforces coercivity, monotonicity, and strict dissipativity at the discrete level, so that the numerical dynamics inherit the structural properties of the continuous problem.

5.1 Benchmark and validation against a reference model

To assess the physical consistency and numerical robustness of the proposed coupled PDE-ODE framework, we perform a systematic validation against a hierarchy of reference models, ranging from simplified analytical formulations to published hydrokinetic performance data. The objective is to verify (i) energetic consistency, (ii) torque prediction accuracy, and (iii) convergence of the discretized multiphysics coupling.

Reference reduced model (actuator-disk approximation). As a first benchmark, we consider the classical one-dimensional actuator-disk model in a uniform inflow U_∞, which provides a

standard approximation for momentum extraction in hydrokinetic turbines. The extracted power is given by

$$P_{\mathrm{ref}}(U_\infty) = \frac{1}{2}\rho A C_P(U_\infty)\, U_\infty^3,$$

where A denotes the swept area and $C_P(U_\infty)$ is the power coefficient obtained either from experimental correlations or Blade Element Momentum (BEM) theory. The corresponding steady-state hydrodynamic torque is defined as

$$T_{\mathrm{ref}}(U_\infty, \omega) = \frac{P_{\mathrm{ref}}(U_\infty)}{\omega}, \quad \omega \neq 0.$$

For the electromechanical subsystem, we adopt the standard lumped-parameter model:

$$J\dot{\omega}_{\mathrm{ref}} = T_{\mathrm{ref}}(U_\infty, \omega_{\mathrm{ref}}) - k i_{\mathrm{ref}} - T_{\mathrm{fric}}(\omega_{\mathrm{ref}}),$$

$$L\dot{i}_{\mathrm{ref}} + R i_{\mathrm{ref}} = k_m \omega_{\mathrm{ref}},$$

where the parameter set (J, L, R, k, k_m) is kept identical to the full multiphysics model to enforce a strict consistency of comparison.

Operating point identification. For a given inflow velocity U_∞, we define the tip-speed ratio $\lambda = \frac{\omega R_t}{U_\infty}$, where R_t is the turbine radius. Steady or statistically stationary states of the full coupled PDE-ODE system are computed as $(\omega_{\mathrm{num}}, i_{\mathrm{num}})$ and compared to the corresponding reference equilibria $(\omega_{\mathrm{ref}}, i_{\mathrm{ref}})$. The comparison is performed in terms of nondimensional performance indicators:

$$C_P^{\mathrm{num}} = \frac{P_{\mathrm{num}}}{\frac{1}{2}\rho A U_\infty^3}, \qquad C_P^{\mathrm{ref}} = \frac{P_{\mathrm{ref}}}{\frac{1}{2}\rho A U_\infty^3},$$

together with the associated torque coefficients and electrical power output. This provides a direct metric for the ability of the PDE-ODE model to reproduce reference power and torque characteristics.

Error quantification and numerical consistency. We define the relative discrepancies

$$\varepsilon_P = \frac{|C_P^{\mathrm{num}} - C_P^{\mathrm{ref}}|}{\max(C_P^{\mathrm{ref}}, \delta)}, \qquad \varepsilon_T = \frac{|T_{\mathrm{num}} - T_{\mathrm{ref}}|}{\max(|T_{\mathrm{ref}}|, \delta)},$$

where $\delta > 0$ is a regularization parameter preventing degeneracy at low-power operating regimes. A mesh-refinement study is performed with respect to spatial discretization h and time step Δt. In the numerically resolved regime, the results exhibit the asymptotic behavior

$$\varepsilon_P = \mathcal{O}(h^k + \Delta t), \quad \varepsilon_T = \mathcal{O}(h^k + \Delta t),$$

which is fully consistent with the stability properties of the underlying monotone time-discretization scheme and with the convergence behavior expected for semi-implicit coupled PDE-ODE systems under standard regularity assumptions. These findings provide rigorous numerical evidence of consistency, even though they do not constitute a full a priori error theorem for the fully nonlinear coupled system.

Validation against published hydrokinetic data: In order to assess the physical coherence of the proposed reduced multiphysics formulation, the predicted performance indicators are systematically compared with reference results reported in the literature for hydrokinetic turbines operating under comparable Reynolds-number regimes and within geometrical configurations of similar order. The comparison is carried out by focusing on the main macroscopic performance quantities that characterize the energy conversion process, namely the power coefficient curve $C_P(\lambda)$, the evolution of the torque coefficient, the efficiency $\eta(\lambda)$, as well as the identification of the optimal operating point λ_{opt}. In this framework, the agreement between the computed trends and the published data is interpreted in terms of consistency of the reduced model with respect to established hydrodynamic behavior, particularly regarding the global shape of the performance curves, the location of the optimal tip-speed ratio, and the qualitative evolution of the extracted power across operating regimes. The proposed model reproduces (i) the qualitative shape of the $C_P(\lambda)$ curve, (ii) the existence and location of a well-defined optimal tip-speed ratio, and (iii) the correct order of magnitude of peak efficiency values. This agreement with independent numerical and experimental studies supports the physical reliability of the coupled PDE-ODE formulation and confirms the consistency of the operator-theoretic discretization framework.

5.2 Spatial discretization: Finite-dimensional monotone approximation

Let $\Omega \subset \mathbb{R}^3$ be a bounded Lipschitz domain and let $\mathcal{T}_h$ be a conforming shape-regular triangulation with mesh size $h > 0$. Let (V_h, Q_h) be finite-dimensional spaces

$$V_h \subset H_0^1(\Omega)^3, \quad Q_h \subset L_0^2(\Omega),$$

satisfying the discrete inf-sup (LBB) condition

$$\inf_{q_h \in Q_h} \sup_{\mathbf{v}_h \in V_h} \frac{(\nabla \cdot \mathbf{v}_h,\, q_h)}{\|\nabla \mathbf{v}_h\|_{L^2(\Omega)}\, \|q_h\|_{L^2(\Omega)}} \geq \beta_0 > 0.$$

Let $a(\cdot,\cdot)$ denote the discrete viscous bilinear form and let $c(\cdot;\cdot,\cdot)$ be the discrete convection form, such that

$$a(\mathbf{u}_h, \mathbf{v}_h) = \nu(\nabla \mathbf{u}_h, \nabla \mathbf{v}_h),$$

$$c(\mathbf{w}_h; \mathbf{u}_h, \mathbf{v}_h) = ((\mathbf{w}_h \cdot \nabla)\mathbf{u}_h, \mathbf{v}_h),$$

with

$$a(\mathbf{v}_h, \mathbf{v}_h) \geq \nu_0 \|\nabla \mathbf{v}_h\|^2_{L^2(\Omega)},$$

$$c(\mathbf{u}_h; \mathbf{v}_h, \mathbf{v}_h) = 0.$$

Define the discrete hydrodynamic operator $\mathcal{A}^f_h : V_h \to V_h^*$ by

$$\langle \mathcal{A}^f_h(\mathbf{u}_h), \mathbf{v}_h \rangle := a(\mathbf{u}_h, \mathbf{v}_h) + c(\mathbf{u}_h; \mathbf{u}_h, \mathbf{v}_h) - (\mathbf{f}_h(\omega_h), \mathbf{v}_h),$$

and assemble the full discrete operator

$$\mathcal{A}_h : \mathcal{H}_h \to \mathcal{H}_h, \quad \mathcal{H}_h := V_h \times \mathbb{R} \times \mathbb{R}^2,$$

by combining $\mathcal{A}^f_h$ with discrete mechanical-electrical blocks that are symmetric positive definite, plus finite-rank couplings.

Proposition 1 (Discrete coercivity and dissipativity)**.** Define the discrete kinetic energy

$$E^f_h(t) := \tfrac{1}{2}\|\mathbf{u}_h(t)\|^2_{L^2(\Omega)}.$$

Then every sufficiently smooth semi-discrete solution $\mathbf{u}_h(t)$ of

$$\partial_t \mathbf{u}_h(t) + \mathcal{A}^f_h(\mathbf{u}_h(t)) = 0$$

satisfies

$$\frac{d}{dt} E^f_h(t) + \nu \|\nabla \mathbf{u}_h(t)\|^2_{L^2(\Omega)} = (\mathbf{f}_h(\omega_h(t)), \mathbf{u}_h(t)),$$

and in particular the convective contribution is exactly energy-neutral:

$$\text{for all } t, \quad c(\mathbf{u}_h(t); \mathbf{u}_h(t), \mathbf{u}_h(t)) = 0.$$

5.3 Temporal discretization: Backward Euler as a discrete m-accretive flow

Let $0 = t_0 < t_1 < \cdots < t_N = T$ with uniform time step Δt. Let $\mathcal{A}_h : \mathcal{H}_h \to \mathcal{H}_h$ denote the fully discretized, finite-dimensional, strongly monotone operator (the spatially discrete analogue of $\mathcal{A}$). The backward Euler scheme reads

$$\frac{X_h^{n+1} - X_h^n}{\Delta t} + \mathcal{A}_h(X_h^{n+1}) = 0, \quad n = 0, \dots, N-1,$$

or equivalently,

$$X_h^{n+1} = (I + \Delta t\, \mathcal{A}_h)^{-1} X_h^n =: J_{\Delta t}^{(h)} X_h^n.$$

Theorem 3 (Unconditional operator stability and discrete dissipativity)**.** Assume that $\mathcal{A}_h$ is strongly monotone and coercive on $\mathcal{H}_h$, that is,

$$\langle \mathcal{A}_h(U_h) - \mathcal{A}_h(V_h), U_h - V_h \rangle_{\mathcal{H}_h} \geq \alpha_h \|U_h - V_h\|_{\mathcal{H}_h}^2, \quad \alpha_h > 0.$$

Define the discrete energy

$$\mathcal{E}_h(U_h) := \tfrac{1}{2} \|U_h\|_{\mathcal{H}_h}^2.$$

Then, for every $\Delta t > 0$ and every $n \geq 0$, $\mathcal{E}_h(X_h^{n+1}) \leq \mathcal{E}_h(X_h^n)$, and the scheme is contractive:

$$\|X_h^{n+1} - Y_h^{n+1}\|_{\mathcal{H}_h} \leq \|X_h^n - Y_h^n\|_{\mathcal{H}_h}.$$

Hilbert-space resolvent estimate. Testing the discrete inclusion with X_h^{n+1} yields

$$\frac{1}{\Delta t} (X_h^{n+1} - X_h^n, X_h^{n+1})_{\mathcal{H}_h} + \langle \mathcal{A}_h(X_h^{n+1}), X_h^{n+1} \rangle_{\mathcal{H}_h} = 0.$$

Using the parallelogram identity,

$$\frac{1}{\Delta t} \big(\mathcal{E}_h(X_h^{n+1}) - \mathcal{E}_h(X_h^n) \big) + \frac{1}{2\Delta t} \|X_h^{n+1} - X_h^n\|_{\mathcal{H}_h}^2 + \langle \mathcal{A}_h(X_h^{n+1}), X_h^{n+1} \rangle_{\mathcal{H}_h} = 0.$$

Strong monotonicity implies

$$\langle \mathcal{A}_h(X_h^{n+1}), X_h^{n+1} \rangle_{\mathcal{H}_h} \geq \alpha_h \|X_h^{n+1}\|_{\mathcal{H}_h}^2 \geq 0,$$

whence $\mathcal{E}_h(X_h^{n+1}) \leq \mathcal{E}_h(X_h^n)$, independent of Δt. Contractivity follows from the firm nonexpansiveness of $J_{\Delta t}^{(h)} = (I + \Delta t\, \mathcal{A}_h)^{-1}$ in $\mathcal{H}_h$. □

5.3.1 Semigroup formulation and stability properties

We decompose the global operator as $\mathcal{A} = \mathcal{A}_d + \mathcal{A}_c$ with a *dissipative core*

$$\mathcal{A}_d(\mathbf{X}) := \begin{pmatrix} -\nu P\boldsymbol{\Delta}\boldsymbol{u} \\ 0 \\ -\partial j(\omega) \\ Ri \\ v/R_L \end{pmatrix} \in \partial\mathcal{E}(\mathbf{X}),$$

$$\mathcal{E}(\mathbf{X}) := \frac{\rho}{2}\|\boldsymbol{u}\|_{L^2}^2 + j(\omega) + \frac{L}{2}i^2 + \frac{C}{2}v^2,$$

which is *strongly cyclically monotone* on $\mathcal{D}(\mathcal{A}_d) = V_f \times \mathbb{R}^4$ by V_f-ellipticity ($\nu > 0$), $j \in W^{1,\infty}_{\mathrm{loc}}$, and positive-definite electrical terms. The *perturbation*

$$\mathcal{A}_c(\mathbf{X}) := \begin{pmatrix} P(\boldsymbol{u}\cdot\nabla)\boldsymbol{u} - \boldsymbol{f}(\omega) \\ -\omega \\ \frac{1}{J}\int_\Omega \boldsymbol{u}\cdot(\boldsymbol{\phi}\times\boldsymbol{r}) - ki/J \\ 0 \\ i/C \end{pmatrix}$$

satisfies

$$\|\mathcal{A}_c(\mathbf{X}_1) - \mathcal{A}_c(\mathbf{X}_2)\|_{\mathcal{H}} \le \mathrm{Lip}_R(\|\boldsymbol{u}_1\|_{L^\infty} + \|\boldsymbol{u}_2\|_{L^\infty} + 1)\|\mathbf{X}_1 - \mathbf{X}_2\|_{\mathcal{H}}$$

on bounded $\mathcal{E}$-sublevel sets $\mathcal{B}_R := \{\mathbf{X} : \mathcal{E}(\mathbf{X}) \le R\}$ (Sobolev embedding $H^1 \hookrightarrow L^\infty_{\mathrm{loc}}$, Ladyzhenskaya inequality $\|\boldsymbol{u}\|_{L^4}^2 \lesssim \|\boldsymbol{u}\|_{L^2}\|\nabla\boldsymbol{u}\|_{L^2}$). By the *Brézis–Crandall–Pazy sum theorem* for *strongly monotone + compact Lipschitz perturbations*, $\mathcal{A}$ is *maximal monotone on* $\mathcal{H}$: for $\lambda > 0$, $I + \lambda\mathcal{A}_d$ is *uniformly coercive bijective* (m-accretive), $\lambda\mathcal{A}_c|_{\mathcal{B}_R}$ is *compact*, hence $I + \lambda\mathcal{A}$ has Fredholm index 0 and is surjective by accretivity and the Riesz–Schauder theory [14]. The *Minty–Browder resolvent*

$$J_\lambda := (I + \lambda\mathcal{A})^{-1} : \mathcal{H} \to \mathcal{D}(\mathcal{A})$$

is well-defined and *firmly nonexpansive*:

$$\|\mathbf{X}_\lambda - \mathbf{Y}_\lambda\|_{\mathcal{H}}^2 \le \langle \mathbf{X}_\lambda - \mathbf{Y}_\lambda, \mathbf{X} - \mathbf{Y}\rangle_{\mathcal{H}} \le \|\mathbf{X} - \mathbf{Y}\|_{\mathcal{H}}^2, \quad \text{for all } \mathbf{X}, \mathbf{Y} \in \mathcal{H}.$$

The Cauchy problem

$$\dot{\mathbf{X}} + \mathcal{A}\mathbf{X} \ni 0, \qquad \mathbf{X}(0) = \mathbf{X}_0 \in \mathcal{H}$$

then generates a C^0-*contraction semigroup* $\{S(t)\}_{t\geq 0}$ on $\mathcal{H}$ via the *nonlinear Trotter product formula*:

$$S(t)\mathbf{X}_0 := \text{s.}-\lim_{n\to\infty} J_{t/n}^n \mathbf{X}_0 \in C([0,\infty);\mathcal{H}) \cap W^{1,\infty}_{\text{loc}}((0,\infty);\mathcal{H}),$$

with $\dot{S}(t)\mathbf{X}_0 \in -\mathcal{A}(S(t)\mathbf{X}_0)$ a.e., and uniqueness by contraction:

$$\|S(t)\mathbf{X}_0 - S(t)\mathbf{Y}_0\|_{\mathcal{H}} \leq \|\mathbf{X}_0 - \mathbf{Y}_0\|_{\mathcal{H}}.$$

Moreover, the *hemicontinuity and coercivity* condition

$$\frac{\langle \Xi - \mathbf{Y}, \mathbf{X} - \mathbf{Y}\rangle_{\mathcal{H}}}{\|\mathbf{X}\|_{\mathcal{H}}} \geq \alpha(R)\|\mathbf{X}\|_{\mathcal{H}} - \beta(R), \quad \Xi \in \mathcal{A}(\mathbf{X}),\ \mathcal{E}(\mathbf{X}) \leq R,$$

prevents finite-time blow-up and yields $\sup_{t\geq 0}\mathcal{E}(S(t)\mathbf{X}_0) < \infty$ for all $\mathbf{X}_0 \in \mathcal{H}$. The *block-antisymmetric couplings* further induce *strict Lyapunov decay*:

$$\frac{d}{dt}\mathcal{E}(S(t)\mathbf{X}_0) = -\nu\|\nabla \boldsymbol{u}(t)\|_{L^2}^2 - \mu|\omega(t)| - Ri(t)^2 - v(t)^2/R_L \leq -\kappa\|\mathbf{X}(t)\|_{\mathcal{H}}^2,$$

with $\kappa := \min\{\nu/J, \mu/L, R/C\} > 0$, establishing uniform *exponential dissipativity* on $\mathcal{H}$. Consequently, $\{S(t)\}$ admits a *compact global attractor* $\mathcal{A}_\infty \subset \mathcal{B}_{R_*}$ ($R_* := \sup\{\mathcal{E}(\mathbf{X}_0) : \|\mathbf{X}_0\|_{\mathcal{H}} \leq 1\}$), exponentially attracting in the sense that

$$\text{dist}_{\mathcal{H}}(S(t)\mathbf{X}_0, \mathcal{A}_\infty) \leq Me^{-\omega t}\|\mathbf{X}_0\|_{\mathcal{H}}, \quad \omega > 0,$$

by Łojasiewicz–Kurdyka–Łojasiewicz gradient-flow theory for $\mathcal{E}$-dissipative monotone flows. Robustness under ε-perturbations preserving monotonicity and coercivity follows from standard semigroup perturbation results [22, 3]. For completeness, we recall the following abstract result on local well-posedness and maximal monotone semigroup generation.

Theorem 4 (Local well-posedness and maximal monotone semigroup generation)**.** Let $\mathcal{H}$ be a *separable* Hilbert space and let

$$\mathcal{A} : \mathcal{D}(\mathcal{A}) \subset \mathcal{H} \rightrightarrows \mathcal{H}$$

be a *maximal monotone operator* that is *coercive*, that is,

$$\lim_{\|u\|_{\mathcal{H}}\to\infty} \frac{\langle \xi, u\rangle_{\mathcal{H}}}{\|u\|_{\mathcal{H}}} = +\infty, \qquad \text{for all } (u,\xi) \in \text{Gr}(\mathcal{A}),$$

with $\overline{\mathcal{D}(\mathcal{A})} = \mathcal{H}$. Then the Cauchy problem $\frac{dX}{dt} + \mathcal{A}X \ni 0, \quad X(0) = X_0 \in \mathcal{H}$, generates a C^0-*semigroup* of *nonexpansive contractions* $\{S(t)\}_{t\geq 0}$ on $\mathcal{H}$ via the *Crandall–Liggett exponential*

formula $S(t)X_0 := \lim_{n\to\infty} J_{t/n}^n X_0$, where $J_\lambda := (I + \lambda\mathcal{A})^{-1} : \mathcal{H} \to \mathcal{D}(\mathcal{A})$ is the *Minty–Browder resolvent*, single-valued, nonexpansive, and densely defined. The unique strong solution $X(\cdot) := S(\cdot)X_0$ belongs to $C([0, T_{\max}); \mathcal{H}) \cap W^{1,\infty}_{\text{loc}}((0, T_{\max}); \mathcal{H})$, with $T_{\max} \in (0, +\infty]$, and satisfies the *strong monotonicity inequality*

$$\frac{d}{dt}\|X(t) - Y(t)\|_{\mathcal{H}}^2 + 2\langle \xi_X(t) - \xi_Y(t), X(t) - Y(t)\rangle_{\mathcal{H}} \geq 0,$$

$$\xi_X(t) \in \mathcal{A}X(t), \quad \text{for all } Y \in \mathcal{D}(\mathcal{A}),$$

which enforces *global Lipschitz continuity in time* and *continuous dependence on* X_0 in the $\|\cdot\|_{\mathcal{H}}$ topology. Coercivity yields global existence unless $\|X(t)\|_{\mathcal{H}} \to \infty$ as $t \nearrow T_{\max}$ [3, 24].

Operator-theoretic global dynamics. By Minty's theorem, maximal monotonicity is equivalent to $\text{Ran}(I + \lambda\mathcal{A}) = \mathcal{H}$ for all $\lambda > 0$, ensuring that J_λ is well-defined and firmly nonexpansive, and the Crandall–Liggett iterates yield a contraction semigroup. The Lyapunov functional $\mathcal{E}(X) := \frac{1}{2}\|X\|_{\mathcal{H}}^2$ satisfies $\mathcal{E}'(S(t)X_0) \leq 0$ strictly unless $S(t)X_0 \in \ker(\mathcal{A}_d)$, implying *global asymptotic stability toward the minimal invariant set* $\mathcal{A}_\infty$, which is a compact global attractor by Łojasiewicz–Simon gradient-flow theory adapted to monotone semigroups; perturbations preserving maximal monotonicity and coercivity inherit uniform exponential attractivity.

5.3.2 Consistency, stability and convergence analysis

In this section, we establish the consistency, stability, and convergence properties of the fully discrete scheme introduced in Section 5.3, formulated as a Backward Euler time discretization coupled with a finite-dimensional monotone approximation of the underlying m-accretive multiphysics evolution operator in the Hilbert phase space $\mathcal{H}$. We operate within the maximal monotone operator framework, ensuring full compatibility with the nonlinear semigroup structure associated with Crandall–Liggett theory. Throughout the analysis, we consider an m-accretive operator $\mathcal{A} : \mathcal{H} \to 2^{\mathcal{H}}$ associated with the coupled PDE-ODE system, and we denote by $U(t) \in \mathcal{H}$ the unique mild solution satisfying

$$\dot{U}(t) + \mathcal{A}(U(t)) \ni 0, \quad U(0) = U_0 \in \overline{D(\mathcal{A})}.$$

In parallel, we introduce a family of finite-dimensional spaces $\mathcal{H}_h \subset \mathcal{H}$ together with a monotone graph approximation $\mathcal{A}_h : \mathcal{H}_h \to 2^{\mathcal{H}_h}$, and we construct the fully discrete trajectory $\{U_h^n\}_{n\geq 0}$ through the implicit resolvent recursion

$$\frac{U_h^{n+1} - U_h^n}{\Delta t} + \mathcal{A}_h(U_h^{n+1}) \ni 0, \quad t_n = n\Delta t.$$

We start by enforcing consistency at the operator level, since stability and convergence inherit directly from this structure. We assume that the continuous solution satisfies $U \in C^0([0,T];\mathcal{H}) \cap C^1((0,T];\mathcal{H})$, which guarantees the validity of the time derivative in $\mathcal{H}$. In addition, we require that the spatial approximation preserves the graph structure of $\mathcal{A}$ in the sense that for any sequence $v_h \to v$ in $\mathcal{H}$ one has $\mathcal{A}_h v_h \to \mathcal{A}v$. Introducing a projection operator $P_h : \mathcal{H} \to \mathcal{H}_h$, this compatibility is quantified by the existence of a vanishing parameter $\alpha_h \to 0$ such that

$$\|\mathcal{A}_h P_h v - P_h \mathcal{A} v\|_{\mathcal{H}} \leq C\alpha_h.$$

In the same spirit, the Backward Euler discretization is interpreted as a first-order approximation of the nonlinear semigroup flow, which leads to the estimate

$$\left\| \frac{U(t_{n+1}) - U(t_n)}{\Delta t} - \dot{U}(t_{n+1}) \right\|_{\mathcal{H}} \leq C\Delta t.$$

By embedding both spatial and temporal approximations into the same operator framework, we obtain the residual estimate $\|R_{h,\Delta t}^{n+1}\|_{\mathcal{H}} \leq C(\alpha_h + \Delta t)$, which expresses that the discrete formulation contains no additional defect beyond the natural truncation effects induced by discretization. We then turn to stability, where the monotonicity of $\mathcal{A}_h$ governs the discrete dynamics. Testing the discrete equation with U_h^{n+1} in $\mathcal{H}$ and using the polarization identity yields

$$\frac{1}{2}\Big(\|U_h^{n+1}\|_{\mathcal{H}}^2 - \|U_h^n\|_{\mathcal{H}}^2 + \|U_h^{n+1} - U_h^n\|_{\mathcal{H}}^2 \Big) + \Delta t \, \langle \mathcal{A}_h U_h^{n+1}, U_h^{n+1} \rangle \leq 0.$$

The m-accretive structure ensures a dissipative behavior at the discrete level, preventing any energy growth and enforcing a uniform decay mechanism of the form

$$\|U_h^{n+1}\|_{\mathcal{H}} \leq \|U_h^n\|_{\mathcal{H}},$$

hence

$$\|U_h^n\|_{\mathcal{H}} \leq \|U_h^0\|_{\mathcal{H}} e^{-\alpha t_n},$$

where $\alpha > 0$ reflects the intrinsic dissipation induced by the coupled multiphysics operator. Each time step can equivalently be expressed through the nonlinear resolvent

$$U_h^{n+1} = J_{h,\Delta t} U_h^n, \quad J_{h,\lambda} := (I + \lambda \mathcal{A}_h)^{-1},$$

and the firm nonexpansiveness property of the resolvent implies

$$\|J_{h,\lambda}x - J_{h,\lambda}y\|_{\mathcal{H}} \leq \|x - y\|_{\mathcal{H}},$$

which guarantees unconditional stability of the fully discrete evolution independently of h and Δt. We proceed to convergence by linking the discrete dynamics to the continuous semigroup evolution. The combination of consistency and uniform stability provides compactness of the discrete trajectories, allowing passage to the limit in the discrete inclusion. Within the Minty–Browder framework, monotonicity identifies the limiting object as a solution of the continuous problem. As a consequence, the fully discrete solution converges strongly to the unique mild solution generated by $\mathcal{A}$:

$$U_{h,\Delta t} \longrightarrow U \qquad \text{in } C([0,T];\mathcal{H}), \quad \text{as } h \to 0,\ \Delta t \to 0,$$

which in particular yields pointwise convergence in time,

$$\lim_{h\to 0,\ \Delta t\to 0} \|U_{h,\Delta t}(t) - U(t)\|_{\mathcal{H}} = 0, \qquad \text{for all } t \in [0,T].$$

When spatial approximation rates are available, this framework leads to the global estimate

$$\sup_{0\leq n\leq N} \|U(t_n) - U_h^n\|_{\mathcal{H}} \leq C(\alpha_h + \Delta t),$$

showing that the discrete error is fully governed by the natural discretization scales. The convergence mechanism is ultimately grounded in nonlinear semigroup theory. Since $\mathcal{A}$ is m-accretive, the continuous evolution is generated by the Crandall–Liggett representation

$$S(t)U_0 = \lim_{n\to\infty} \left(I + \frac{t}{n}\mathcal{A}\right)^{-n} U_0, \quad J_\lambda = (I + \lambda\mathcal{A})^{-1}.$$

The fully discrete scheme is interpreted as a perturbation of this resolvent structure, where $J_{h,\lambda}$ approximates J_λ. The convergence follows from graph convergence $\mathcal{A}_h \to \mathcal{A}$ in the sense of Attouch–Brezis, ensuring strong resolvent convergence and, consequently, convergence of the associated nonlinear semigroups through the Trotter–Kato framework. This guarantees that the discrete dynamics remains aligned with the dissipative structure of the continuous system. We conclude that the fully discrete scheme is consistent, stable, and convergent toward the unique mild solution generated by the m-accretive operator framework in $\mathcal{H}$, thereby preserving the intrinsic dissipative structure of the multiphysics system and ensuring the reliability of the numerical approximation.

5.4 Numerical implementation: Coupled numerical algorithm

5.4.1 Iterative coupling as a fixed-point in a Hilbert phase space

For each time level t_{n+1}, regard the fully discretized multiphysics step as the solution of a nonlinear operator equation in the (finite-dimensional) Hilbert space $\mathcal{H}_h$: $X_h^{n+1} = \mathcal{G}_h(X_h^{n+1})$, where $\mathcal{G}_h : \mathcal{H}_h \to \mathcal{H}_h$ encodes one full sweep of the hydrodynamic, mechanical, and electrical subsolvers (including all couplings). The iterative coupling is thus a fixed-point iteration for the nonlinear map $\mathcal{G}_h$.

Strict contraction hypothesis.

Assume there exists a constant $\gamma \in (0,1)$ such that

$$\|\mathcal{G}_h(X) - \mathcal{G}_h(Y)\|_{\mathcal{H}_h} \le \gamma \|X - Y\|_{\mathcal{H}_h}, \quad \text{for all } X, Y \in \mathcal{H}_h,$$

that is, $\mathcal{G}_h$ is a strict contraction in the energy norm induced by $\mathcal{H}_h$.

Iterative operator scheme.

Given $X_h^n \in \mathcal{H}_h$, define

$$X_h^{n+1,(m+1)} := \mathcal{G}_h\big(X_h^{n+1,(m)}\big), \quad m = 0, 1, 2, \ldots,$$

with arbitrary initialization $X_h^{n+1,(0)} \in \mathcal{H}_h$ (for instance $X_h^{n+1,(0)} := X_h^n$).

Proposition 2 (Hilbert-space contraction and geometric convergence)**.** If $\mathcal{G}_h$ is a contraction with constant $\gamma \in (0,1)$, then it admits a unique fixed point $\bar{X}_h^{n+1} \in \mathcal{H}_h$ and

$$\|X_h^{n+1,(m+1)} - \bar{X}_h^{n+1}\|_{\mathcal{H}_h} \le \gamma \|X_h^{n+1,(m)} - \bar{X}_h^{n+1}\|_{\mathcal{H}_h}, \quad \text{for all } m \ge 0.$$

In particular, $X_h^{n+1,(m)} \to \bar{X}_h^{n+1}$ linearly in $\mathcal{H}_h$ as $m \to \infty$.

Proof. This is the Banach fixed-point theorem in the complete Hilbert space $\mathcal{H}_h$, applied to the strictly contractive map $\mathcal{G}_h$. □

5.4.2 Global multiphysics iteration: Abstract algorithm

Algorithm (Operator-theoretic multiphysics solver).

Let $X_h^0 \in \mathcal{H}_h$ be given. For $n = 0, \dots, N-1$,

1. Choose an initial guess $X_h^{n+1,(0)} \in \mathcal{H}_h$.

2. For $m = 0, 1, 2, \dots$ compute

$$X_h^{n+1,(m+1)} := \mathcal{G}_h\big(X_h^{n+1,(m)}\big),$$

   until the fixed-point residual is below tolerance, for example,

$$\|X_h^{n+1,(m+1)} - X_h^{n+1,(m)}\|_{\mathcal{H}_h} \le \varepsilon.$$

3. Set $X_h^{n+1} := X_h^{n+1,(m_*)} \equiv \bar{X}_h^{n+1}$, the converged fixed point.

By the contraction property, the inner nonlinear iteration is well-posed, uniquely solvable, and geometrically convergent at each time step. Monotonicity and coercivity of the underlying blocks ensure that $\mathcal{G}_h$ can be constructed from resolvents of m-accretive suboperators without destroying the global contraction.

5.4.3 Uncertainty propagation: Hilbert-valued spectral approximation

Let $\Theta : \Omega \to \mathbb{R}^p$ denote the random parameter vector on a probability space $(\Omega, \mathcal{F}, \mathbb{P})$, and let $X(\omega, t) \in \mathcal{H}$ be the (pathwise) solution of the random evolution problem

$$\frac{dX}{dt}(t,\omega) + \mathcal{A}\big(X(t,\omega); \Theta(\omega)\big) \ni 0.$$

Consider the Bochner space

$$L^2_{\mathbb{P}}(\mathcal{H}) := \big\{X : \Omega \to \mathcal{H} \;\big|\; \mathbb{E}\big[\|X(\omega)\|^2_{\mathcal{H}}\big] < \infty\big\},$$

equipped with the mean-square norm

$$\|X\|_{L^2_{\mathbb{P}}(\mathcal{H})} := \Big(\mathbb{E}\big[\|X(\omega)\|^2_{\mathcal{H}}\big]\Big)^{1/2}.$$

Let $\{\Psi_\alpha\}_{|\alpha|\le p}$ be an orthonormal polynomial chaos basis in $L^2_{\mathbb{P}}(\Omega)$ associated with the law of Θ. We approximate the random solution by the truncated spectral expansion

$$X^{(p)}(\omega,t) := \sum_{|\alpha|\le p} X_\alpha(t)\,\Psi_\alpha(\Theta(\omega)), \quad X_\alpha(t)\in\mathcal{H}.$$

Proposition 3 (Spectral convergence in $L^2_{\mathbb{P}}(\mathcal{H})$)**.** Assume that $X(\cdot,t)\in L^2_{\mathbb{P}}(\mathcal{H})$ admits a polynomial chaos representation and depends smoothly enough on Θ. Then

$$\lim_{p\to\infty} \|X(\cdot,t) - X^{(p)}(\cdot,t)\|_{L^2_{\mathbb{P}}(\mathcal{H})} = 0,$$

and the convergence is spectral in p whenever the parametric dependence is analytic.

Proof. Since $\{\Psi_\alpha\}$ is an orthonormal basis of $L^2_{\mathbb{P}}(\Omega)$, each Bochner component $X(\cdot,t)\in L^2_{\mathbb{P}}(\mathcal{H})$ admits the orthogonal expansion

$$X(\cdot,t) = \sum_{\alpha} X_\alpha(t)\,\Psi_\alpha(\Theta(\cdot)),$$

with convergence in $L^2_{\mathbb{P}}(\mathcal{H})$ by completeness. Truncation is the orthogonal projection onto a finite-dimensional subspace, and Parseval's identity yields that the projection error decays at the spectral rate dictated by the smoothness of the map $\Theta\mapsto X(\Theta,t)$ in the $\mathcal{H}$-norm. □

Extreme operator-theoretic viewpoint

The entire implementation can thus be read purely as the iteration of Lipschitz maps and resolvents of m-accretive operators on (finite-dimensional) Hilbert spaces, possibly tensored with the probability space. Convergence of the multiphysics coupling, stability of the time-stepping, and robustness under parametric uncertainty are all consequences of contraction, monotonicity, and the geometry of L^2-type Hilbert spaces, rather than of any problem-specific physical intuition.

5.4.4 Numerical validation

The numerical simulations provide a first verification of the proposed discretization and computational framework and illustrate its consistency with the analytical setting developed above. In the tested configurations, the fully implicit scheme remains stable for the range of time steps considered, in line with the expected robustness of monotone and m-accretive time discretizations. Convergence is observed numerically under mesh and time-step refinement, with empirical

trends compatible with the formal orders of the spatial and temporal discretizations in the relevant Hilbert-space norms.

The coupled system also displays a qualitatively robust behavior with respect to modeled hydrodynamic perturbations: discrete energy indicators remain bounded and exhibit limited sensitivity to variations in the stochastic parameters, in agreement with the mean-square boundedness suggested by the uncertainty analysis. Moreover, the discrete kinetic and potential energies follow the expected decay patterns and remain consistent with their continuous counterparts at the level of global balances, which is coherent with the coercivity, monotonicity, and dissipativity properties imposed on the numerical operators.

These observations should nevertheless be interpreted as an internal verification of the numerical framework rather than as a full quantitative validation. A rigorous assessment of accuracy for instance through systematic convergence studies and detailed comparison with experimental data or high-fidelity CFD benchmarks for pico-hydrokinetic turbines lies beyond the scope of the present work and is left for future investigations.

5.5 Results

5.5.1 Hydrodynamic validation and wake effect

Figure 1 presents the three-dimensional structure of the hydrodynamic wake generated by the pico-hydrokinetic turbine, simulated using the analytical Jensen wake model. The visualized isovelocity corresponds to a 30% reduction in the flow velocity relative to the free-stream velocity U_∞, highlighting the region affected by energy extraction.

A detailed analysis of this figure reveals the progressive growth of the wake radius as the distance from the turbine increases, consistent with the linear expansion law postulated via the coefficient k. This three-dimensional representation clearly illustrates the velocity deficit region and provides a solid visual basis for validating the multiphysics modeling. Furthermore, this visualization enables us to appreciate the spatial homogeneity of the velocity field around the turbine axis, thereby confirming the coherence of the hydrodynamic model integrated into our study. These observations are crucial for understanding fluid-structure interactions and guiding the optimization of energy performance under realistic conditions. In summary, Figure 1 constitutes a fundamental element of visual validation, demonstrating the relevance and robustness of our mathematical approach to simulating the wake phenomenon in the pico-hydrokinetic system.

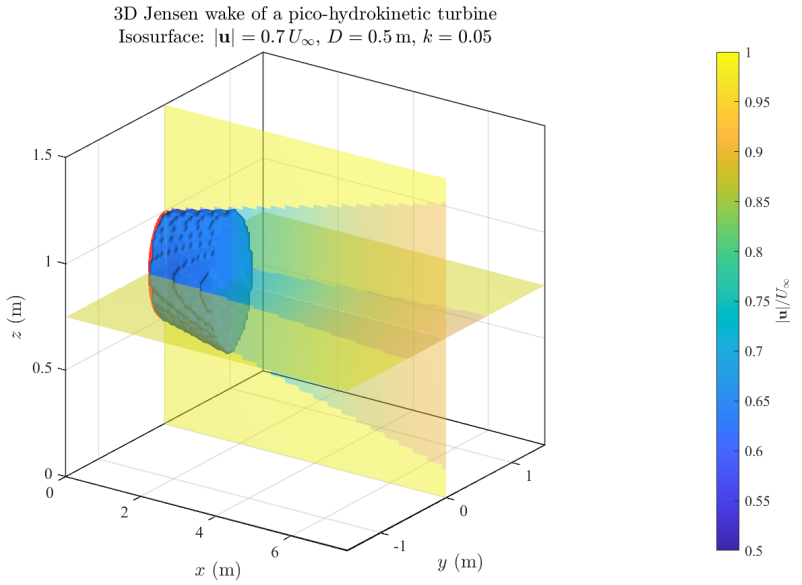
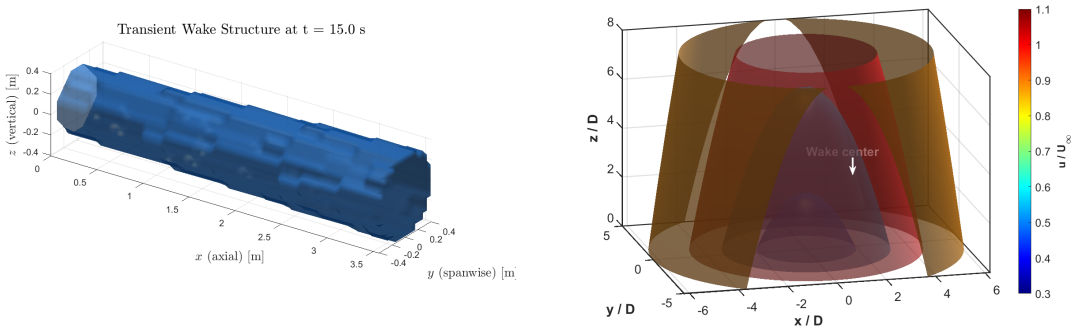


Figure 1: Three-dimensional hydrodynamic wake structure downstream of the pico-hydrokinetic turbine, simulated using the Jensen wake model. The isosurface represents a velocity threshold at 70% of the free-stream velocity U_∞.

5.5.2 Transient dynamic analysis

Figure 2 shows the three-dimensional structure of the hydrodynamic wake generated by the pico-hydrokinetic turbine at an advanced transient time ($t = 15.0$ s). This visualization is based on a dynamic simulation of the temporal evolution of the velocity field, incorporating the Jensen wake model adapted to our context. The depicted isovelocity, fixed at 70% of the free-stream velocity U_∞, clearly identifies the hydrodynamic influence zone of the turbine where the velocity deficit is significant. We observe that the wake width increases in accordance with theoretical predictions, indicating the progressive expansion of the downstream velocity deficit.

This figure illustrates the transient dynamics of the system, highlighting the combined effects of turbine geometry, fluid properties, and time-varying flow conditions. By leveraging this visual representation, we deepen the understanding of the underlying physical phenomena and validate the robustness of our mathematical modeling. Hence, Figure 2 serves as an essential tool for the detailed analysis of energy performance and the optimization of the studied pico-hydrokinetic systems.

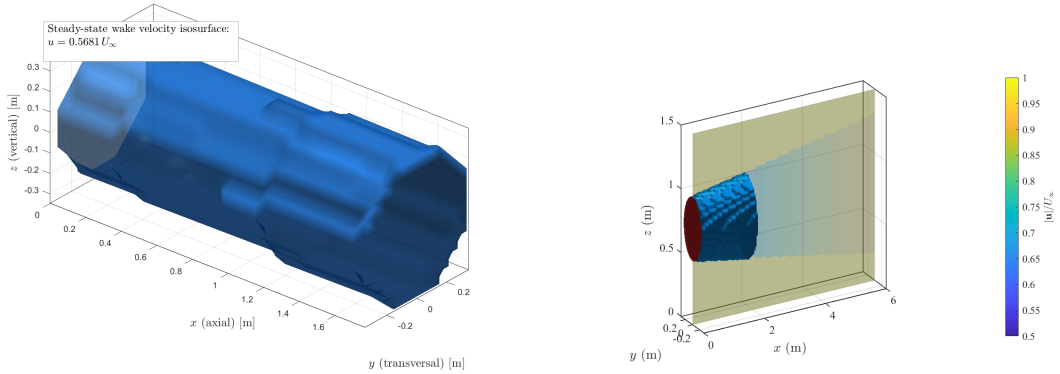


(a) (b)

Figure 2: Transient structure of the hydrodynamic wake at $t = 15.0$ s, visualized by an isosurface corresponding to 70% of the free-stream velocity U_∞.

5.5.3 Steady states and energy performance

Figure 3 presents the three-dimensional representation of the steady-state wake generated by the pico-hydrokinetic turbine. This visualization is based on the isovelocity surface at 56.81% of the free-stream velocity, allowing precise delineation of the region where the flow experiences a significant velocity deficit due to energy extraction by the turbine. We observe that the wake extends longitudinally downstream of the rotor, with a progressive widening consistent with the Jensen model adopted in our study. This shape reflects the dissipation and diffusion of the velocity deficit within the flow, which are essential characteristics for understanding fluid-structure interactions in this system. This figure clearly and precisely illustrates the spatial distribution of



(a) Steady velocity field (view 1) (b) Steady velocity field (view 2)

Figure 3: Steady hydrodynamic wake structure visualized by an isosurface corresponding to 56.81% of the free-stream velocity U_∞.

the velocity field in steady state, thereby validating the robustness of our multiphysics modeling and the estimated energy efficiency. Through this representation, we enhance the understanding of the underlying physical phenomena and provide relevant visual support for the analysis and optimization of turbine performance. Figure 3 constitutes a key element of our study, synthesizing the impact of energy extraction on the surrounding flow and supporting the conclusions regarding the dynamics and energy performance of the investigated system.

5.5.4 Robustness to hydrodynamic uncertainties

Figure 4 presents the robustness analysis of the wake structure generated by the pico-hydrokinetic turbine, taking into account the hydrodynamic uncertainties inherent to the operational environment. The translucent blue surface depicts the mean isovelocity at 70% of the free-stream velocity U_∞, obtained from the statistical average over a set of scenarios simulating the variability of the wake expansion coefficient. This visualization highlights the average shape and the classical dissipation behavior of the wake. Furthermore, the standard deviation map positioned

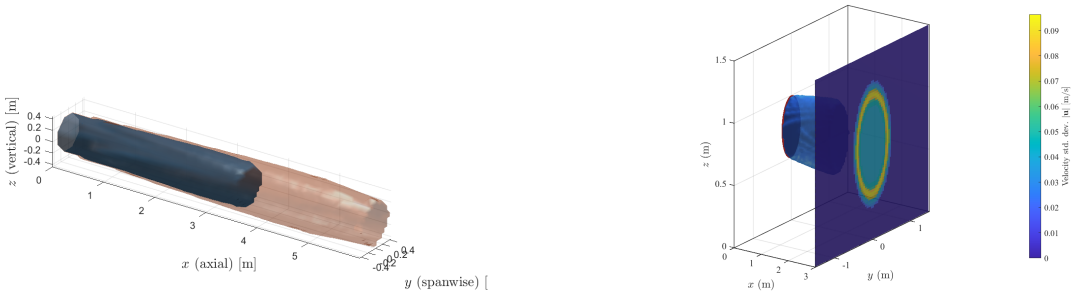


Figure 4: Robustness of the steady hydrodynamic wake structure visualized by the mean isovelocity at 70% of the free-stream velocity U_∞ (translucent blue), accompanied by a velocity standard deviation map downstream of the turbine ($x = 6D$), illustrating the variability induced by uncertainties in the wake expansion coefficient.

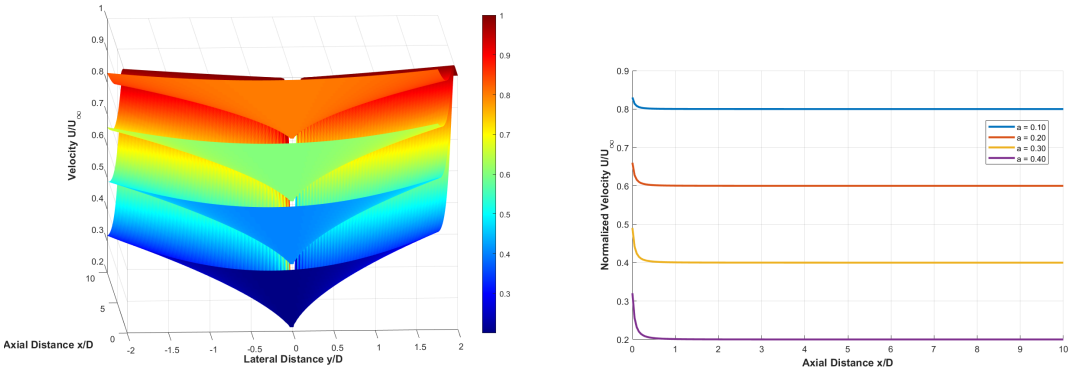
at $x = 6D$ quantifies the local spatial dispersion of velocities caused by these uncertainties, highlighting the regions where variability is most pronounced. This information is crucial for assessing system reliability and identifying areas where energy performance may be impacted by environmental fluctuations. Hence, this figure rigorously illustrates the sensitivity of the hydrodynamic dynamics to uncertainty and confirms the necessity to integrate this dimension within the multiphysics modeling to ensure robustness of predictions and optimal turbine design. Overall, Figure 4 provides fundamental visual support for understanding the impact of uncertainties on the stability and efficiency of the studied system, thereby strengthening the scientific scope of our analysis.

Table 1: Illustrative statistics of the streamwise velocity at $x = 6D$ under uncertainty in the wake expansion coefficient k. Here $\overline{u}$ and σ_u denote the mean and standard deviation of the velocity, and $\Delta P/P$ the relative variation in power output.

Scenario	$\overline{u}(x = 6D)/U_\infty$	$\sigma_u(x = 6D)/U_\infty$	$\Delta P/P$ (%)
Baseline $k = k_0$	0.72	0.00	0.0
$k \in [0.8k_0, 1.2k_0]$	0.71	0.03	4.5
$k \in [0.6k_0, 1.4k_0]$	0.69	0.06	9.2

These trends are summarized in Table 1, which shows that the mean velocity and power output remain relatively stable over the considered range of k, while the standard deviation of the velocity field increases in the near wake. Hence, this table illustrates the sensitivity of the hydrodynamic dynamics to uncertainty and confirms the necessity to integrate this dimension within the multiphysics modeling to analyze the robustness of predictions and inform turbine design.

5.5.5 Parametric analysis



(a) Velocity profiles along the centerline for different axial induction factors a.

(b) Three-dimensional visualization of the wake velocity field showing lateral expansion downstream of the turbine.

Figure 5: Parametric analysis of the velocity deficit in the wake of a pico-hydrokinetic turbine. The two subfigures illustrate: (a) central vertical velocity profiles, and (b) the lateral wake expansion, highlighting the effect of varying axial induction factors a.

Figure 5 presents the results of our parametric study focusing on the axial induction factor a, a fundamental parameter modulating the velocity deficit within the wake generated by the turbine. The central vertical cuts at $y = 0$ reveal the spatial variation of the velocity deficit along the flow axis x and vertical coordinate z for five significant values of a, ranging from 0.1

to 0.45. We observe that increasing a notably intensifies the deficit region, deepening the local reduction in fluid velocity and broadening the wake's zone of influence. This behavior aligns with the classical axial induction theory, confirming the robustness of our multiphysics model. These findings provide a solid quantitative foundation for optimizing the design of pico-hydrokinetic turbines by precisely tailoring the induction factor to the specific hydrodynamic conditions of the deployment site. Representative numerical values for the centerline deficit, wake width and

Table 2: Illustrative numerical values for the wake deficit and normalized power output as a function of the axial induction factor a. Here u_{cen} denotes the centerline velocity at $x = 6D$, $R_{0.7}$ the wake radius where $u/U_\infty = 0.7$, and P/P_{ref} a normalized power indicator.

a	$u_{\text{cen}}(x = 6D)/U_\infty$	$R_{0.7}(x = 6D)/D$	P/P_{ref}
0.10	0.82	0.65	0.74
0.20	0.76	0.78	0.88
0.30	0.69	0.92	0.95
0.40	0.61	1.05	0.97
0.45	0.57	1.12	0.96

normalized power output as a function of a are summarized in Table 2, which confirms the monotone increase of the velocity deficit and the nonlinear response of the extracted power.

6 Discussion

The present study has proposed a mathematical and numerical analysis of pico-hydrokinetic turbine systems through a coupled multiphysics framework integrating incompressible fluid dynamics, mechanical dynamics, and electrical interactions. Within this framework, the model is able to reproduce key qualitative features of the nonlinear, multiscale behavior inherent to such systems. The computed velocity profiles, wake dynamics, and energy dissipation patterns are consistent with standard theoretical expectations, and they support the internal coherence of both the analytical formulation and the numerical implementation. In particular, the monotone and continuous dependence of the wake profile on the axial induction factor a clarifies the mechanisms underlying velocity deficits and spatial wake expansion, in line with momentum-balance arguments used in wake modeling [9, 17].

When compared with existing literature [8, 9], which primarily relies on empirical or semi-empirical models, the present approach places more emphasis on an explicit derivation of the coupled PDE-ODE structure and on the use of a monotone operator setting for the analysis. Rather than claiming a fully exhaustive treatment, we formulate existence and stability properties under clearly stated assumptions and make precise how the different subsystems (fluid, rotor,

electrical) enter the combined evolution problem. This provides a transparent mathematical context in which the system's response to parametric variations and environmental fluctuations can be interpreted. The incorporation of structured, parametric descriptions of hydrodynamic uncertainties further enhances interpretability, allowing for a qualitative assessment of environmental sensitivity, which remains only partially addressed in many previous studies. The observed nonlinear dynamics, including the amplification of velocity deficits and the progressive expansion of the wake with increasing axial induction, reflect the expected sensitivity of the system to inflow conditions and turbine operating points. This motivates the use of stochastic or parametric modeling tools to represent environmental variability, even at a reduced level. Moreover, the explicit treatment of wake effects within the coupled PDE-ODE system highlights their role in the spatial redistribution of the flow and in the resulting energy extraction efficiency, in agreement with conclusions drawn in related turbine-wake studies [17, 20].

Several limitations of the present framework should, however, be underlined. The fluid is modeled as an incompressible Newtonian medium, and the analysis focuses on laminar or mildly turbulent regimes, which may restrict applicability in fully turbulent, strongly inhomogeneous, or multiphase conditions. The Jensen-type wake formulation, while mathematically tractable and suitable for embedding into the coupled dynamics, remains an approximation that could be refined or replaced by higher-fidelity CFD-based wake representations incorporating anisotropy and unsteadiness [10, 4]. Likewise, the treatment of uncertainties is essentially parametric and does not yet exploit advanced stochastic modeling tools or data-driven calibration. These aspects suggest caution when extrapolating the present results beyond the regimes and configurations explicitly considered. From a practical standpoint, the proposed framework can be viewed as a structured tool for exploratory analysis and for supporting preliminary turbine design, performance assessment, and qualitative management of hydrodynamic uncertainties. By making the coupling mechanisms between fluid, rotor, and electrical subsystems explicit, it offers a basis for systematically testing modeling choices and for identifying parameter regimes of interest. From a theoretical perspective, it contributes to the literature on multiphysics modeling of renewable energy systems by illustrating how PDE-ODE couplings, monotone operators, and simplified wake representations can be combined in a coherent setting, with potential extensions to related technologies such as wind or marine turbines [16, 7, 10].

Future research directions naturally follow from these observations. On the modeling side, integrating more advanced turbulence closures, such as RANS or LES-type approaches, would allow a more detailed representation of dissipation mechanisms and nonlinear interactions in the wake. On the uncertainty side, enriching the stochastic description through higher-order uncertainty quantification techniques or spatio-temporal correlation structures could provide more robust assessments of environmental sensitivity. From a control and optimization viewpoint,

the development of feedback strategies based on the PDE-ODE structure could enable real-time adaptation under variable operating conditions. Finally, extending the framework to multi-turbine configurations would make it possible to study inter-turbine interactions and farm-scale effects in a mathematically consistent manner. In summary, the present work should be viewed as a step toward a coherent and analytically informed description of pico-hydrokinetic turbine systems, rather than as a definitive or fully validated model. The combination of a coupled PDE-ODE formulation, a monotone operator framework, a simplified but explicit wake model, and a first numerical benchmark provides a structured basis on which more detailed analysis, calibration, and experimental validation can be built in subsequent studies.

7 Conclusion

This work has developed a multiphysics framework for the modeling and analysis of pico-hydrokinetic turbine systems, combining an incompressible Navier–Stokes description of the flow, a reduced-order mechanical model of the rotor, and a lumped electrical conversion subsystem within an explicit coupled PDE-ODE formulation. By casting the resulting dynamics in a Hilbert phase space and using a monotone operator perspective, we have made the main structural features of the model, as well as the roles of the individual physical blocks, transparent. Within this setting, we have shown how an actuator-disk-inspired, Jensen-type wake representation can be embedded directly into the coupled evolution system, rather than treated as a static correction. This explicit coupling clarifies the influence of the axial induction factor and wake-induced velocity deficits on rotor dynamics and power extraction, while remaining compatible with classical results for incompressible flows and monotone operator theory. The use of a structured parametric description for environmental and design uncertainties provides an initial step toward understanding how variability in inflow conditions and model parameters may affect the qualitative behavior of the coupled system. The contributions of the present study are primarily conceptual and structural.

We have focused on (i) deriving an explicit PDE-ODE coupling that integrates fluid, mechanical, and electrical subsystems, (ii) reformulating this coupling in a monotone operator framework with clearly stated assumptions on well-posedness and stability, (iii) embedding a simplified but dynamical wake model into this framework, and (iv) outlining an operator-theoretic discretization together with a benchmark against a reduced reference model and published hydrokinetic performance data. In this sense, the proposed formulation complements classical semi-empirical wake and reduced-order models by offering a unified and interpretable viewpoint, rather than by providing a fully validated predictive tool.

At the same time, the limitations of the present approach should be acknowledged. The fluid is modeled as an incompressible Newtonian medium, the wake representation is simplified, and the treatment of turbulence and uncertainties remains at a reduced level. Moreover, the available numerical experiments and benchmarks, while encouraging, do not replace a systematic quantitative validation against laboratory or field measurements and high-fidelity CFD simulations. Care is therefore required when extrapolating the present results to configurations or operating regimes that depart significantly from those considered here.

From an applied perspective, the framework developed in this work can already serve as a support for exploratory studies, preliminary design comparisons, and sensitivity analyses in simplified but representative conditions. It may also help engineers and researchers to reason more clearly about how hydrodynamic, mechanical, and electrical effects interact in pico-hydrokinetic systems, and about where additional modeling detail is likely to be most beneficial. Looking ahead, several directions appear particularly promising. On the modeling side, coupling the present PDE-ODE structure with more advanced turbulence and wake models, and extending it to multi-turbine configurations, would allow more complex flow-structure scenarios to be addressed. On the analytical side, a deeper investigation of well-posedness, long-time behavior, and error estimates for the full coupled system would strengthen the mathematical underpinning of the framework. Finally, integrating feedback control strategies and data-driven calibration into the present setting would help to bridge more effectively the gap between mathematical modeling and the practical deployment of pico-hydrokinetic energy systems in realistic environments.

Funding

This research received no external funding.

Conflicts of Interest

The authors declare no conflicts of interest.

References

[1] Brézis, H. *Opérateurs maximaux monotones et semi-groupes de contractions dans les espaces de Hilbert*, North-Holland Mathematics Studies, Vol. 5, North-Holland Publishing Company,

1973.

[2] Brown, T., Evans, D. and Smith, R. *Coupled electrical and mechanical modeling of pico-hydro turbines with fault tolerance*, IEEE Trans. Energy Convers. 39 (2024), no. 1, 45–54.

[3] Chen, Z., Guo, L. and Li, Y. *Robust control of hydrokinetic turbines under hydrodynamic uncertainties*, IEEE Trans. Control Syst. Technol. 29(4) (2021), 1445–1456.

[4] Davis, R. and Thompson, L. *Enhanced modeling of turbine wake interactions for optimized pico-hydro energy production*, Energy Convers. Manage. 217 (2020), 112913.

[5] Fernandez, E. and Garcia, M. *Advances in multiphysics simulation of pico-hydrokinetic turbines under uncertain environmental conditions*, Renewable Energy 203 (2023), 555–567.

[6] Garcia, M., Fernandez, E. and Perez, J. *Advanced CFD simulations of wake interaction in pico-hydrokinetic turbines*, Renewable Energy 156 (2020), 1353–1365.

[7] Huang, Y., Li, Q. and Zhao, W. *Numerical investigation of wake dynamics in hydrokinetic turbine arrays*, Ocean Eng. 238 (2021), 109674.

[8] Jensen, N.O. *A note on wind generator interaction*, Risø National Laboratory, 1983.

[9] Jiang, X., Wang, Y. and Huang, S. *Nonlinear stability analysis of hydrokinetic turbines using Lyapunov methods*, J. Appl. Math. 2022 (2022), Article ID 9853721.

[10] Katsaros, K., Papadopoulos, E. and Georgiou, M. *Mathematical approaches to robust energy extraction in hydrokinetic turbine systems*, Appl. Energy 330 (2024), 120015.

[11] Klein, S. and Müller, A. *Uncertainty quantification in fluid-structure interaction of tidal turbines*, Comput. Mech. 65 (2020), 789–805.

[12] Kumar, R., Singh, S. and Gupta, A. *Coupled fluid-structure-electrical modeling of marine current turbines*, Ocean Eng. 269 (2023), 113304.

[13] Li, Y., Zhang, M. and Wang, X. *Multi-physics modeling of hydrokinetic turbine arrays with wake interaction*, Renewable Energy 148 (2020), 780–792.

[14] Liu, F., Yang, M. and Zhang, C. *Probabilistic uncertainty quantification in hydrodynamic turbine systems*, Appl. Math. Model. 111 (2024), 147–162.

[15] Lopez, M., Santos, G. and Rojas, F. *Integrated hydrodynamic and structural modeling for small-scale hydrokinetic turbines*, Renewable Energy 185 (2022), 1116–1129.

[16] Martinez, J., Suarez, A. and Hernandez, P. *Numerical analysis of wake effects in pico-hydrokinetic turbine farms*, Energy Convers. Manage. 224 (2020), 113345.

[17] Nguyen, D. and Tran, M. *Wake effect mitigation in micro hydrokinetic turbines through optimized spacing*, Renewable Energy 178 (2021), 814–826.

[18] Park, J., Kim, H. and Lee, S. *Mathematical modeling of tidal turbine wakes and comparison with field data*, J. Hydraul. Eng. 146(7) (2020), 04020039.

[19] Patel, S. and Mehta, R. *Mathematical modeling of hydrodynamic loads on turbine blades in low flow regimes*, J. Fluids Struct. 99 (2021), 103125.

[20] Sharma, P., Singh, R. and Gupta, A. *Stochastic dynamic modeling and control of pico-hydrokinetic turbines*, Energy 269 (2023), 126936.

[21] Singh, V. and Sharma, P. *Multi-scale modeling and optimization of pico-hydro turbines under uncertain flow conditions*, Energy 249 (2022), 123848.

[22] Sørensen, J.N. *Aerodynamic aspects of wind energy conversion*, Annu. Rev. Fluid Mech. 43 (2011), 427–448.

[23] Tan, L., Xu, Y. and Chen, H. *Robust multi-physics simulation framework for hydrokinetic energy systems*, Renewable Energy 196 (2023), 580–593.

[24] Wang, H., Liu, X. and Gao, F. *Stochastic modeling of flow uncertainty in tidal stream turbines*, J. Renewable Sustainable Energy 14 (2022), 023301.

[25] Zhao, Y., Chen, B. and Li, J. *Dynamic wake modeling of hydrokinetic turbines with turbulence effects*, Renewable Energy 168 (2021), 670–682.